



# 1 Mapping and Assessing Variability in the Antarctic Marginal Ice Zone, 2 the Pack Ice and Coastal Polynyas

3 Julienne C. Stroeve<sup>1,2</sup>, Stephanie Jenouvrier<sup>3,4</sup>, G. Garrett Campbell<sup>1</sup>, Christophe Barbraud<sup>4</sup> and  
4 Karine Delord<sup>4</sup>

5 <sup>1</sup>National Snow and Ice Data Center, Cooperative Institute for Research in Environmental  
6 Sciences, University of Colorado, Boulder, CO, USA

7 <sup>2</sup>Center for Polar Observation and Modelling, University College London, London, UK

8 <sup>3</sup>Woods Hole Oceanographic Institution, Woods Hole, MA, USA

9 <sup>4</sup>Centre d'Etudes Biologiques de Chizé, UMR 7372 CNRS, 79360 Villiers en Bois, France

10

## 11 Abstract

12 Sea ice variability within the marginal ice zone (MIZ) and polynyas plays an important role for  
13 phytoplankton productivity and krill abundance. Therefore mapping their spatial extent, seasonal and  
14 interannual variability is essential for understanding how current and future changes in these biological  
15 active regions may impact the Antarctic marine ecosystem. Knowledge of the distribution of different  
16 ice types to the total Antarctic sea ice cover may also help to shed light on the factors contributing  
17 towards recent expansion of the Antarctic ice cover in some regions and contraction in others. The long-  
18 term passive microwave satellite data record provides the longest and most consistent data record for  
19 assessing different ice types. However, estimates of the amount of MIZ, consolidated pack ice and  
20 polynyas depends strongly on what sea ice algorithm is used. This study uses two popular passive  
21 microwave sea ice algorithms, the NASA Team and Bootstrap to evaluate the distribution and variability  
22 in the MIZ, the consolidated pack ice and coastal polynyas. Results reveal the NASA Team algorithm has  
23 on average twice the MIZ and half the consolidated pack ice area as the Bootstrap algorithm. Polynya  
24 area is also larger in the NASA Team algorithm, and the timing of maximum polynya area may differ by  
25 as much as 5 months between algorithms. These differences lead to different relationships between sea  
26 ice characteristics and biological processes, as illustrated here with the breeding success of an Antarctic  
27 seabird.

## 28 1. Introduction

29 Changes in the amount of the ocean surface covered by sea ice play an important role in  
30 the global climate system. For one, sea ice and its snow cover have a high surface reflectivity,  
31 or albedo, reflecting the majority of the sun's energy back to space. This helps to keep the polar  
32 regions cool and moderates global climate. When sea ice melts or retreats, the darker (lower  
33 albedo) ocean is exposed, allowing the ocean to absorb solar energy and warm, which in turn  
34 melts more ice, creating a positive feedback loop. During winter, sea ice helps to insulate the  
35 ocean from the cold atmosphere, influencing the exchange of heat and moisture to the  
36 atmosphere with impacts on cloud cover, pressure distribution and precipitation. These in turn



37 can lead to large-scale atmospheric changes, affecting global weather patterns [e.g. *Jaiser et*  
38 *al.*, 2012]. Sea ice also has important implications for the entire polar marine ecosystem,  
39 including sea ice algae, phytoplankton, crustaceans, fish, seabirds, and marine mammals, all of  
40 which depend on the seasonal cycle of ice formation in winter and ice melt in summer. For  
41 example, sea ice melt stratifies the water column, producing optimal light conditions for  
42 stimulating bloom conditions that Antarctic sea birds rely upon for their breeding success and  
43 survival [e.g. *Park et al.*, 1999].

44 In stark contrast to the Arctic, which is undergoing a period of accelerated ice loss in the last  
45 several decades [e.g. *Stroeve et al.*, 2012; *Serreze and Stroeve*, 2015], the Antarctic is  
46 witnessing a modest increase in total sea ice extent [*Parkinson and Cavalieri*, 2012]. Sea ice  
47 around Antarctica reached another record high extent in September 2014, recording a  
48 maximum extent of more than 20 million km<sup>2</sup> for the first time since the modern passive  
49 microwave satellite data record began in October 1978. This follows previous record maxima in  
50 2012 and 2013, resulting in an overall increase in Antarctic September sea ice extent of 1.1%  
51 per decade since 1979. While the observed increase is statistically significant, Antarctic's sea  
52 ice extent (SIE) is also highly variable from year to year and region to region [e.g. *Maksym et*  
53 *al.*, 2012; *Parkinson et al.*, 2012; *Stammerjohn et al.*, 2012]. The temporal variability is  
54 underscored by sea ice conditions in 2015 when the winter ice cover returned back to the 1981-  
55 2010 long-term mean. Also, recent sea ice assessments from early satellite images from the  
56 Nimbus program of the late 1960s indicate similarly high but variable SIE as observed over  
57 2012-2014 [*Meier et al.*, 2013; *Gallaher et al.*, 2014]. Mapping of the September 1964 ice edge  
58 indicates that ice extent likely exceeded both the 2012 and 2013 record monthly-average  
59 maximums, at 19.7±0.3 million km<sup>2</sup>. This was followed in August 1966 by an extent estimated at  
60 15.9±0.3 million km<sup>2</sup>, considerably smaller than the record low maximum extent of the modern  
61 satellite record (set in 1986). The circumpolar average also hides contrasting regional variability,  
62 with some regions showing either strong positive or negative trends with magnitudes equivalent  
63 to those observed in the Arctic [*Stammerjohn et al.*, 2012]. In short, interannual and regional  
64 variability in Antarctic sea ice is considerable, and while the current positive trend in circumpolar  
65 averaged Antarctic sea ice extent is important, it is not unprecedented compared to  
66 observations from the 1960s and it is not regionally distributed.

67 Several explanations have been put forward to explain the positive Antarctic sea ice trends.  
68 Studies point to anomalous short-term wind patterns that both grow and spread out the ice,  
69 related to the strength of the Amundsen Sea low pressure [e.g. *Turner et al.*, 2013; *Reid et al.*,  
70 2015]. Other studies suggest melt water from the underside of floating ice surrounding the  
71 continent has risen to the surface and contributed to a slight freshening of the surface ocean  
72 [e.g. *Bintanja et al.*, 2012]. While these studies have helped to better understand how the ice,  
73 ocean and atmosphere interact, 2012 to 2014 showed different regions and seasons  
74 contributing to the net positive sea ice extent, which has made it difficult to establish clear links  
75 and suggests that no one mechanism can explain the overall increase.

76 While the reasons for the increases in total extent remain poorly understood, it is likely that  
77 these changes are not just impacting total sea ice extent but also the distribution of pack ice, the  
78 marginal ice zone and polynyas. The marginal ice zone (MIZ) is a highly dynamic region of the



79 ice cover defined by the transition between the open ocean and the consolidated pack ice. In  
80 the Antarctic, wave action penetrates hundreds of kilometers into the ice pack, resulting in small  
81 rounded ice floes from wave-induced fracture [Kohout *et al.*, 2014]. Thus, in contrast to the  
82 Arctic, ocean waves primarily define the dynamic MIZ region, though in the Arctic this may be  
83 changing as the Arctic continues to experience longer and larger ice-free summers with  
84 increased fetch on the later-timed ice edge advance [Wang *et al.*, 2015]. This in turn makes the  
85 MIZ region particularly sensitive to both atmospheric and oceanic forcing, such that during  
86 quiescent conditions, it may consist of a diffuse thin ice cover, with isolated thicker ice floes  
87 distributed over a large (hundreds of kilometers) area. In contrast, during high on-ice wind and  
88 wave events, the MIZ region contracts to a compact ice edge with rafted ice pressed together in  
89 front of the solid ice pack. In general, ocean waves define the dynamic MIZ region, where ice  
90 floes are relatively small due to wave-induced fracture. The smaller the ice floes, the more  
91 mobile they are and large variability in ice conditions can be found in response to changing wind  
92 and ocean conditions. Polynyas on the other hand are open water areas near the continental  
93 margins that often remain open as a result of strong katabatic winds flowing down the Antarctic  
94 plateau. The winds continually push the newly formed sea ice away from the continent, which  
95 influences the outer ice edge as well, thus contributing to the overall increase in total ice extent  
96 in specific regions around the Antarctic continent where katabatic winds are persistent.

97 Both polynyas and the MIZ are biologically important regions of the sea ice cover that have  
98 important implications for the entire trophic web, from primary productivity [Yun *et al.*,  
99 submitted], to top predator species, such as seabirds. Near the ice edge and in the MIZ, the  
100 stable upper layer of the water column is optimal for phytoplankton production [e.g. Park *et al.*  
101 1999]. This phytoplankton bloom is subsequently exploited by zooplankton, with effects that  
102 cascade up to fish, seabirds and marine mammals. Similarly, within polynyas there is a narrow  
103 opportunity for phytoplankton growth, the timing of which plays an important role in both  
104 biogeochemical cycles [Smith and Barber, 2007] and biological production [Arrigo and van  
105 Dijken, 2003; Ainley *et al.*, 2010]. However, while studies have suggested that the timing of sea  
106 ice retreat is synchronized with the timing of the phytoplankton bloom, other factors such as  
107 wind forcing [Chiswell, 2011], thermal convection [Ferrari, 2014] and iron availability [Boyd *et al.*,  
108 2007, and references therein] play important roles as well.

109 In this study we use the long-term passive microwave sea ice concentration data record to  
110 evaluate variability and trends in the marginal ice zone, the pack ice and polynyas from 1979 to  
111 2014. A complication arises however as to which sea ice algorithm to use. There are at least a  
112 dozen algorithms available, spanning different time-periods, which give sea ice concentrations  
113 that are not necessarily consistent with each other [see Ivanova *et al.*, 2015; 2014 for more  
114 information]. To complicate matters, different studies have used different sea ice algorithms to  
115 examine sea ice variability and attribution. For example, Hobbs and Raphael [2010] used the  
116 Had1SST1 sea ice concentration data set [Rayner *et al.*, 2003], which is based on the NASA  
117 Team algorithm [Cavalieri *et al.*, 1999], whereas Raphael and Hobbs [2014] relied on the  
118 Bootstrap algorithm [Comiso and Nishio, 2008]. To examine the influence in the choice of sea  
119 ice algorithm on the results, we use both the Bootstrap and NASA Team sea ice algorithms.  
120 Results are evaluated hemispheric-wide and also for different regions. We then discuss the  
121 different implications resulting from the two different satellite estimates for biological impact



122 studies. We focus on the breeding success of snow petrels because seabirds have been  
123 identified as useful indicators of the health and status of marine ecosystems [Piatt and  
124 Sydeman, 2007].

## 125 2. Data and Methods

126 To map different ice types, the long-term passive microwave data record is used, which  
127 spans several satellite missions, including the Scanning Multichannel Microwave Radiometer  
128 (SMMR) on the Nimbus-7 satellite (October 1978 to August 1987), the Special Sensor  
129 Microwave/Imager (SSM/I) sensors -F8 (July 1987 to December 1991), -F11 (December 1991  
130 to September 1995), -F13 (May 1995 to December 2007) and the Special Sensor Microwave  
131 Imager/Sounder (SSMIS) sensor -F17 (January 2007- to present), both on the Defense  
132 Meteorological Satellite Program's (DMSP) satellites. Derived sea ice concentrations (SICs)  
133 from both the Bootstrap (BT) [Comiso and Nishio, 2008] and the NASA Team (NT) sea ice  
134 algorithms [Goersen *et al.*, 1992; Cavalieri *et al.*, 1999] are available from the National Snow  
135 and Ice Data Center (NSIDC) and provide daily fields from October 1978 to present, gridded to  
136 a 25 km polar stereographic grid. While a large variety of sea ice concentration algorithms are  
137 available, the lack of good validation has made it difficult to determine which algorithm provides  
138 the most accurate results during all times of the year and for all regions. Using two algorithms  
139 provides a consistency check on variability and trends.

140 Using these SIC fields, we define six binary categories of sea ice based on different SIC  
141 thresholds [Table 1]. Because the marginal ice zone is highly dynamic in time and space, it is  
142 difficult to precisely define this region of the ice cover. Wadhams [1986] defined the MIZ as that  
143 part of the ice cover close enough to the open ocean boundary to be impacted by its presence,  
144 e.g. by waves. Thus the MIZ is typically defined as the part of the sea ice that is close enough to  
145 the open ocean to be heavily influenced by waves, and it extends from the open ocean to the  
146 dense pack ice. In this study, we define the MIZ as extending from the outer sea ice/open ocean  
147 boundary (defined by  $SIC \geq 0.15$  ice fraction) to the boundary of the consolidated pack ice  
148 (defined by  $SIC = 0.80$ ). This definition was previously used by Strong and Rigor [2013] to  
149 assess MIZ changes in the Arctic and matches the upper sea ice concentration limit used by the  
150 National Ice Center in mapping the Arctic MIZ. The consolidated ice pack is then defined as the  
151 area south of the MIZ with ice fractions between  $0.80 \leq SIC \leq 1.0$ . Coastal polynyas are defined  
152 as regions near the coast that have  $SIC < 0.80$ .

153 To automate the detection of different ice types, radial transects from 50 to 90S are  
154 individually selected to construct one-dimensional profiles [Figure 1]. The algorithm first steps  
155 from the outer edge until the 0.15 SIC is detected, providing the latitude of the outer MIZ edge.  
156 Next, the algorithm steps from the outer MIZ edge until either the 0.80 SIC is encountered, or  
157 the continent is reached. Data points along the transect between these SIC thresholds are  
158 flagged as the MIZ. In this way, the MIZ includes an outer band of low sea ice concentrations  
159 that surrounds a band of inner consolidated pack ice, *but* sometimes the MIZ also extends all  
160 the way to the Antarctic coastline (as sometimes observed in summer). South of the MIZ, the  
161 consolidated ice pack ( $0.80 \leq SIC \leq 1.0$ ) is encountered; however, low sea ice concentrations  
162 can appear near the coast inside the pack ice region as well. These are areas of potential



163 coastal polynyas. While it is difficult to measure the fine scale location of a polynya at 25km  
164 spatial resolution, the lower sea ice concentrations provide an indication of some open water  
165 near the coast, which for sea birds provides a source of open water for foraging. Using our  
166 method of radial transects, the algorithm then steps from the coast northward and flags pixels  
167 with  $< 0.80$  SIC until a  $0.80$  SIC pixel appears and defines that region as a potential coastal  
168 polynya. Within the consolidated pack ice (and away from the coast), it is also possible to  
169 encounter instances where  $0.15 < \text{SIC} < 0.80$  or  $\text{SIC} < 0.15$ . These are flagged as open pack  
170 ice and open water areas within the consolidated pack ice, respectively. Finally, an ocean mask  
171 derived from climatology and distributed by NSIDC was applied to remove spurious ice  
172 concentrations at the ice edge as a result of weather effects.

173 **Figure 2** shows sample images of the classification scheme as applied to the NASA Team  
174 and Bootstrap algorithms on days 70 and 273, respectively, in 2013. During the fall and winter  
175 months when the ice cover is expanding there is a well-established consolidated pack ice  
176 region, surrounded by the outer MIZ. Coastal polynyas are also found surrounding the continent  
177 in both algorithms. As will be discussed in more detail in the results section, the BT algorithm  
178 tends to show a larger consolidated ice pack than NT, particularly during the timing of maximum  
179 extent. During the melt season there is mixing of low and high ice concentrations, leading to  
180 mixtures of different categories, which is still seen to some extent in the March images.  
181 However, during March areas of polynyas (green), open water (pink) and open pack ice  
182 (orange) appear to extend from the coastline in some areas (e.g. southern Weddell and Ross  
183 seas). While any pixel with  $\text{SIC} < 0.8$  adjacent to the coastal boundary is flagged as potential  
184 polynya when stepping northwards, if a pixel is already flagged as MIZ or consolidated pack ice  
185 when stepping southwards, it remains flagged as MIZ or pack ice. After that analysis, a check  
186 for pixels with SICs less than  $0.8$  is done to flag for broken ice or open water. Thus, during these  
187 months (e.g. December to February or March), the physical interpretation of the different ice  
188 classes may be less useful.

189 Using the binary classification scheme, gridded fields and regional averages are computed.  
190 We show results for the entire Antarctic sea ice cover, as well as for six different regions as  
191 defined previously by *Parkinson and Cavalieri* [2012]. These regions are shown in **Figure 3** for  
192 reference. Climatological mean daily and monthly time-series spanning 1981 to 2010 are  
193 computed for each region and for each ice classification together with the  $\pm$  one standard  
194 deviation ( $1\sigma$ ). Monthly trends over the entire time-series are computed by first averaging the  
195 daily fields into monthly values and then using a standard linear least squares, with statistical  
196 significance evaluated at the 90<sup>th</sup>, 95<sup>th</sup> and 99<sup>th</sup> percentiles using a student t-test.

## 197 3. Results

### 198 3.1 Seasonal Cycle

#### 199 3.1.1 Circumpolar Extent

200 We begin with an assessment of the consistency of the outer ice edge between both sea ice  
201 algorithms [**Figure 4**]. As a result of the large emissivity difference between open water and sea  
202 ice, estimates of the outer ice edge location has high consistency between the two algorithms



203 despite having large differences in sea ice concentration [e.g. *Ivanova et al.*, 2014; 2015]. This  
204 therefore results in similar total sea ice extents between both algorithms during all calendar  
205 months, and similar long-term trends. This is where the similarities end however.

206 **Figure 5** summarizes the climatological mean seasonal cycle in the extent of the different  
207 ice categories listed in Table 1 for both sea ice algorithms, averaged for the total hemispheric-  
208 wide Antarctic sea ice cover. The one standard deviation is given by the colored shading. The  
209 first notable result is that the BT algorithm has a larger consolidated ice pack than the NT  
210 algorithm, which comes at the expense of a smaller MIZ. Averaged over the entire year, the  
211 NASA Team MIZ area is twice as large as that in the Bootstrap algorithm [see also **Table 2**].  
212 The BT algorithm additionally has a smaller spatial extent of potential coastal polynyas and little  
213 to no broken ice or open water within the consolidated pack ice. Another important result is that  
214 the BT algorithm exhibits less interannual variability in the different ice types, as illustrated by  
215 the smaller standard deviations from the long-term mean (e.g. the shading). Thus, while the  
216 total extents are not dissimilar between the algorithms, how that ice is distributed among the  
217 different ice categories differs quite substantially as well as their year-to-year variability.

218 The timing of the ice edge advance and retreat are generally similar in both algorithms,  
219 reflecting the fact that both algorithms do well in distinguishing open water from sea ice. In  
220 regards to the consolidated pack ice, it advances in March, with the BT algorithm showing a  
221 distinct peak in September, reaching a maximum extent of  $14.89 \cdot 10^6 \text{ km}^2$ . The NT algorithm  
222 shows a somewhat broader peak, extending from July to October, with the peak extent also  
223 reached in September. In September the NT pack ice extent is a little more than twice the  
224 spatial extent of the MIZ;  $11.31 \cdot 10^6 \text{ km}^2$  vs.  $5.41 \cdot 10^6 \text{ km}^2$  [Table 2]. BT on the other hand has a  
225 much smaller fraction (41% less) of ice classified as MIZ ( $3.19 \cdot 10^6 \text{ km}^2$ ). In both algorithms the  
226 MIZ also begins to expand in March, and continues to expand until November or December,  
227 after which it rapidly declines. However, in the NT algorithm, an initial peak in MIZ coverage is  
228 also reached around September, coinciding with the peak in the consolidated pack ice extent  
229 and stays nearly constant until the end of November. The further increase in the MIZ coverage  
230 after the consolidated ice pack begins to retreat implies that as the pack ice begins to retreat, it  
231 does so in part by first converting to MIZ over a wider area. This is consistent with the idea that  
232 in spring, the pack ice on average undergoes divergence first (in relation to the circumpolar  
233 trough being poleward and south of the ice edge, as reflected by the Semi-Annual Oscillation,  
234 SAO, of the trough). This in turn facilitates increased solar heating of open water areas, which in  
235 turn facilitates increased melt back, thus creating, eventually, a more rapid ice edge retreat (in  
236 Nov-Dec) as compared to the slow ice edge advance in autumn [see *Watkins and Simmonds*,  
237 1999].

238 Open pack ice is negligible in the Bootstrap algorithm except for a slight peak in  
239 November/December. With the NASA Team algorithm however there is a clear increase in open  
240 pack ice during the ice expansion phase, which continues to increase further as the pack ice  
241 begins to retreat, also peaking in November. Open pack ice in September contributes another  
242  $1.28 \cdot 10^6 \text{ km}^2$  to the total Antarctic sea ice extent in the NT algorithm, compared to only  $0.36 \cdot 10^6$   
243  $\text{km}^2$  in the BT algorithm. As with the open pack ice, the fraction of potential coastal polynyas  
244 also increases during the ice expansion phase, and then continues to increase as the sea ice



245 retreats, peaking around November in the NT algorithm, with a total area of  $1.02 \cdot 10^6 \text{ km}^2$ , and in  
246 December in BT ( $0.81 \cdot 10^6 \text{ km}^2$ ). Inner open water within the pack is generally only found  
247 between November and March in both algorithms as the total ice cover retreats and reaches its  
248 seasonal minimum.

### 249 3.2.2 Regional Analysis

250 Analysis of the Antarctic-wide sea ice cover however is of limited value given that the sea  
251 ice variability and trends are spatially heterogeneous [Makysm *et al.*, 2012]. For example, while  
252 the ice cover is increasing in the Ross Sea, it has at the same time decreased in the  
253 Bellingshausen/ Amundsen Sea region. Thus, we may anticipate significant regional variability  
254 in the amount, seasonal cycle and trends of the different ice classes (trends discussed in  
255 section 3.3). The Ross Sea for example [Figure 6, top] consists of a large fraction of  
256 consolidated ice throughout most of the year (April through November) in both algorithms, with  
257 considerably less MIZ. In the Bellingshausen/Amundsen Sea on the other hand [Figure 6, 2<sup>nd</sup>  
258 row], the NT algorithm has a MIZ extent that exceeds that of the consolidated pack ice until  
259 May, after which the spread ( $\pm 1\sigma$ ) in MIZ and consolidated pack ice overlaps. The reverse is  
260 true in the BT algorithm, which consistently indicates a more consolidated ice pack, with only  
261  $0.51 \cdot 10^6 \text{ km}^2$  flagged as MIZ during the maximum extent in September, compared to  $0.84 \cdot 10^6$   
262  $\text{km}^2$  in the NT algorithm. On an annual basis, the NT algorithm shows about equal proportion of  
263 MIZ and consolidated pack ice in the Bellingshausen/Amundsen Sea whereas, the BT algorithm  
264 indicates a little more than a third of the total ice cover is MIZ. In the Ross Sea there is also a  
265 very broad peak in the maximum extent of the consolidated pack ice, stretching between July  
266 and October in the NT algorithm, and a peak in MIZ extent in late August/early September with  
267 a secondary peak in December as the pack ice continues to retreat. The BT algorithm shows a  
268 similar broad peak in the pack ice extent, but with less interannual variability, and a nearly  
269 constant fraction of MIZ throughout the advance and retreat of the pack ice. Annually the NT  
270 algorithm shows about 56% more MIZ in the Ross Sea than the BT algorithm. Note that in both  
271 algorithms, the pack ice retreats rapidly after the maximum extent is reached.

272 In the Weddell Sea, the pack ice extent advances in March in both algorithms and peaks in  
273 August in the NT algorithm, September in BT. The MIZ also begins its expansion in March and  
274 continues to increase until September in NT, and then again until December (both algorithms)  
275 as the pack ice quickly retreats [Figure 6 (middle)]. In this region, the sea ice expands  
276 northwards until it reaches a region with strong winds and currents. The open pack ice north of  
277 the pack ice continues to expand either by further freezing or breaking of the pack ice by the  
278 winds and currents. Overall, the Weddell Sea has the largest spatial extent in the MIZ in both  
279 algorithms, as well as the largest distribution of pack ice. In the NT algorithm however, the MIZ  
280 extent within the Weddell Sea is again considerably larger than in the BT algorithm. For  
281 example, in September the NASA Team algorithm gives a climatological mean MIZ extent of  
282  $1.61 \cdot 10^6 \text{ km}^2$ , twice as large as that in the Bootstrap algorithm ( $0.83 \cdot 10^6 \text{ km}^2$ ).

283 Finally, in the Indian and Pacific Ocean sectors [Figure 6, 4<sup>th</sup> row] the MIZ extent increases  
284 from March until November in both algorithms, retreating about a month after the peak extent in  
285 the pack ice is reached. However, in the Pacific Ocean sector [Figure 6, bottom], the MIZ  
286 comprises a larger percentage of the overall ice cover, being nearly equal in spatial extent in the



287 NASA Team algorithm, and even exceeding that of the pack ice in September (0.93 (MIZ) vs.  
288  $0.76 \cdot 10^6 \text{ km}^2$  (pack ice)). This results in an annual mean extent of MIZ that exceeds that of the  
289 consolidated pack ice. This is the only region of Antarctica where this occurs. In the BT  
290 algorithm, the reverse is true, with again a larger annual extent of pack ice than MIZ.

291 While the above discussion focused on regional differences in the MIZ and the consolidated  
292 pack ice, the spatial extent and timing of coastal polynyas also varies between the algorithms.  
293 For example, in the Bellingshausen/Amundsen sea region, the maximum polynya area occurs in  
294 July in NT ( $0.17 \cdot 10^6 \text{ km}^2$ ) and in December in the BT algorithm ( $0.11 \cdot 10^6 \text{ km}^2$ ). Thus, while the  
295 overall maximum spatial extent in polynya area is not all that different in the two algorithms, the  
296 timing of when the maximum is reached differs by 5 months. This is also the case in the Pacific  
297 Ocean where the NASA Team algorithm reaches its largest spatial extent in polynya area in  
298 August ( $0.14 \cdot 10^6 \text{ km}^2$ ) whereas the Bootstrap shows the maximum polynya area occurring in  
299 November ( $0.11 \cdot 10^6 \text{ km}^2$ ). In other regions, such as the Indian Ocean, the Ross Sea and the  
300 Weddell Sea, the timing of the maximum polynya area occurs similarly in both algorithms,  
301 during November for the Indian Ocean and December in the Ross and Weddell Seas. The Ross  
302 and Weddell seas have the largest climatological polynya areas,  $0.32$  (NT)/ $0.26$  (BT)  $10^6 \text{ km}^2$   
303 and  $0.33$  (NT)/ $0.30$  (BT)  $10^6 \text{ km}^2$ , respectively.

## 304 3.2 Trends

### 305 3.2.1 Spatial Expansion/Contraction during September

306 As mentioned earlier, estimates of the outer ice edge location are similar between both  
307 algorithms. This is also true in terms of the locations where the outer edge is expanding or  
308 contracting. A way to illustrate this is shown in **Figure 7 (top)**, which shows a spatial map of the  
309 trend in the outer edge of the entire ice pack (defined as the 15% SIC contour, equivalent to the  
310 total sea ice extent) for both algorithms during the month of September, the month at which the  
311 ice pack generally reaches its maximum extent. Locations of northward expansion (red areas)  
312 and contraction (blue areas) are remarkably consistent between algorithms as well as the  
313 spatial extent of the expansion and contraction. In both algorithms the ice edge shows trends  
314 towards expansion within the Ross Sea, the Amundsen Sea and the Pacific and Indian Ocean  
315 sectors, except for the Davis Sea, where there is a trend towards contraction of the outer ice  
316 edge. The Bellingshausen and Weddell seas also show trends towards contraction of the outer  
317 ice edge.

318 While there is general consistency between the algorithms in both the location and changes  
319 of the outer ice edge over time, there are differences as to how the MIZ and pack ice widths are  
320 changing [**Figure 7, middle and bottom**]. In the BT algorithm, the MIZ width is a relatively  
321 constant ring around the edge of the consolidated pack ice, with little change over time. Thus, in  
322 the BT algorithm, the spatial pattern of expansion/contraction of the total ice cover in September  
323 is largely a result of the changes happening in the pack ice [Figure 7, bottom]. The NT algorithm  
324 on the other hand shows more pronounced changes in the MIZ, such that both the MIZ and the  
325 pack ice contribute to the observed spatial patterns and changes in the total ice cover. However,  
326 expansion/contraction of the MIZ and pack ice in the NT algorithm sometimes counter act each  
327 other. For example the contraction of the total ice edge the Bellingshausen Sea is a result of  
328 contraction of the consolidated ice pack while the MIZ width is generally increasing as a result of





329 the MIZ moving further towards the continent. This is also true in the Weddell Sea and the  
330 Indian Ocean.

331 Somewhat surprisingly, the spatial pattern of expansion/contraction of the MIZ is broadly  
332 similar between both algorithms, despite overall smaller changes in the BT algorithm. This  
333 highlights the fact that the spatial trends in SIC are similar to the spatial trends in SIE as well as  
334 to the timing of advance/retreat/duration, so that the spatial trends in the MIZ and pack ice will  
335 show the same overall pattern because they rely on SIC. This also highlights the fact that the  
336 spatial pattern persists throughout the regional ice covered area, i.e. from the edge to the  
337 coastal area, which may imply that climate-related regional wind-driven changes at the ice edge  
338 are felt all the way to the coast. Alternatively it may imply that the ocean is also responding to  
339 the same climate-related wind changes, thus communicating the change all the way to the  
340 coast.

### 341 3.2.2 Circumpolar and Regional Daily Trends

342 **Figure 8** summarizes daily circumpolar Antarctic trends in the pack ice, MIZ and polynyas  
343 for both algorithms, with monthly mean trends listed in **Table 3**. Both algorithms are broadly  
344 similar during the ice expansion phase, indicating positive trends in the consolidated ice pack  
345 and mostly negative trends in the MIZ until the pack ice reaches its peak extent. Thus, during  
346 these months, the positive trends in total SIE are a result of expansion of the consolidated pack  
347 ice. However, during retreat of the pack ice, trends in the MIZ switch to positive in the NASA  
348 Team algorithm while remaining mostly negative in the Bootstrap algorithm. At the same time,  
349 daily trends in the pack ice become noisy in the NT algorithm, alternating between positive and  
350 negative trends while trends remain positive in the BT algorithm. Table 3 indicates that the  
351 positive trends in the consolidated pack during the ice expansion/retreat phase (March through  
352 November) are statistically significant ( $p < 0.01$ ) for the BT algorithm, and from March to July in  
353 the NT algorithm ( $p < 0.05$ ). Trends in the MIZ are not statistically significant, except during  
354 September and October at the 90% confidence level in the NT algorithm. Trends in the pack ice  
355 are larger in the BT algorithm, particularly in August through November, in part reflecting a  
356 shrinking MIZ whereas the NT algorithm shows positive trends in the MIZ during those months.  
357 Trends in possible polynyas near the continent are negative throughout most of the year in both  
358 algorithms, except for December and January. However, none of the polynya trends are  
359 statistically significant.

360 Regionally, there are larger differences between the two algorithms, in particular with  
361 regards to the MIZ as already alluded to in Figure 7. To highlight the regional differences Figure  
362 9 shows daily trends as a function longitude (x-axis) and month (y-axis) for the pack ice (top),  
363 the MIZ (middle) and coastal polynyas (bottom). Monthly trends averaged for each of the 5  
364 sectors are also listed in Table 3. Focusing first on the pack ice trends, we find the spatial  
365 patterns of positive and negative trends are generally consistent between both algorithms,  
366 though the magnitudes of the trends tend to be larger in the Bootstrap algorithm, which in turn  
367 impacts the statistical significance of the trends (see also Table 3). For example, in the Ross  
368 Sea, the largest regional positive trends in total SIE are found at a rate of 119,000 km<sup>2</sup> per  
369 decade [e.g. Turner *et al.*, 2015], accounting for about 60% of the circumpolar ice extent  
370 increase. In the BT algorithm this is entirely a result of large positive trends in the pack ice from



371 March to November ( $p < 0.01$ ). While the Ross Sea sector trends from the NT algorithm are  
372 spatially consistent with the pack ice trends shown in the BT algorithm, trends are only  
373 statistically from April to June ( $p < 0.05$ ). Instead, statistically significant positive trends in the MIZ  
374 dominate August to October in the NT algorithm, which is also the season with the largest  
375 overall trends in the SIE in this region (e.g. Spring). This would suggest perhaps different  
376 interpretation of processes impacting the overall ice expansion in the Ross Sea depending on  
377 which algorithm is used. Several studies have suggested a link between sea ice anomalies in  
378 the Ross Sea and the wind-field associated with the Amundsen Sea Low (ASL) [e.g. *Fogt et al.*,  
379 2012; *Hosking et al.*, 2013; *Turner et al.*, 2012]. The strengthened southerly winds over the  
380 Ross Sea cause a more compacted and growing consolidated ice cover in the BT algorithm at  
381 the expense of a shrinking MIZ, whereas in the NT algorithm the area of the MIZ is increasing  
382 more than the pack ice during autumn, which may additionally suggest an oceanic influence.  
383 While this is true as averaged over the entire Ross Sea sector, Figure 9 highlights that the area-  
384 averaged trends hide spatial variability, with positive trends in the MIZ in the eastern part of the  
385 Ross Sea and negative trends in the western part.

386 While the magnitude of pack ice trends are generally larger in the Bootstrap algorithm, there  
387 are some exceptions. For example, in the Weddell Sea, the NT algorithm exhibits larger  
388 negative trends in the pack ice between June and November whereas the BT algorithm shows  
389 mixed positive and negative trends of smaller magnitude. This is also true with regards to MIZ  
390 trends during these months. However, none of the trends are statistically significant. In the  
391 Weddell Sea, expansion of the overall ice cover is only statistically significant during the autumn  
392 months (MAM) [e.g. *Turner et al.*, 2015]. During this time-period, both algorithms agree on  
393 statistically significant positive trends in the pack ice area, that extend through May for the NT  
394 algorithm ( $p < 0.05$ ) and through June for the BT algorithm ( $p < 0.05$ ). Statistically significant  
395 trends are also seen during March in the MIZ and polynya area ( $p < 0.05$ ), with larger trends in  
396 the NT algorithm ( $p < 0.01$ ). Thus, overall expansion of sea ice in the Weddell during autumn is in  
397 part driven by expansion of the MIZ early in the season, after which it is controlled by further  
398 expansion of the consolidated pack.

399 In contrast, the Bellingshausen/Amundsen Sea is a region undergoing declines in the overall  
400 ice cover [e.g. *Parkinson and Cavalieri*, 2012; *Stammerjohn et al.*, 2012]. Separating out trends  
401 for both the pack ice and the MIZ reveals negative trends in the consolidated pack ice during the  
402 start of ice expansion in March and April and also during initial retreat (September and October)  
403 in both algorithms, though none of the trends are statistically significant [Table 3]. This is the  
404 only region where the BT algorithm does not show statistically significant trends in the pack ice.  
405 Negative trends are also found in the MIZ during the initial ice advance phase in both algorithms  
406 though again none of them are statistically significant. Interestingly, during June and July, the  
407 NT algorithm shows large positive trends in the pack ice ( $p < 0.01$ ) at the expense of negative  
408 trends in the MIZ, though the MIZ trends are not statistically significant and are smaller than the  
409 positive trends in the pack ice. While the MIZ trends are not statistically significant, these results  
410 are consistent with the observation that the SIE trends in the Bellingshausen/Amundsen Sea  
411 are largely wind-driven, so it would be expected that the wind-driven compaction would lead to  
412 decreased MIZ and increased pack ice. Finally, both algorithms indicate statistically significant



413 positive trends in coastal polynyas during November for this region (with larger trends in the NT  
414 algorithm,  $+1,000 \text{ km}^2\text{a}^{-1}$  ( $p<0.05$ ) and  $+600 \text{ km}^2\text{a}^{-1}$  ( $p<0.10$ ), respectively).

415 Finally, in the Pacific and Indian Oceans we again see spatial consistency in pack ice and  
416 MIZ trends for both algorithms, with generally larger (smaller) pack ice (MIZ) trends for the BT  
417 algorithm, though trends are closer in magnitude in the Pacific sector from March to July. The  
418 BT algorithm indicates statistically significant trends in the pack ice from March to November in  
419 both sectors ( $p<0.05$ ), while trends in overall SIE are only statistically significant in the Indian  
420 Ocean during MAM and JJA. The inconsistency in statistical significance between total SIE and  
421 pack ice trends is likely a result of corresponding negative trends in the MIZ, particularly in the  
422 Pacific sector, though the negative BT MIZ trends are not statistically significant. The NT  
423 algorithm mostly has statistically significant trends in the pack ice during the initial expansion  
424 phase only ( $p<0.05$ ). In the Indian Ocean, there are also significant positive trends in MIZ during  
425 March ( $p<0.05$ ) and April ( $p<0.10$ ) and also June and July ( $p<0.10$ ) that would contribute  
426 towards overall positive SIE trends. Both algorithms suggest an increase in polynya area from  
427 March to May ( $p<0.05$ ) in the Pacific sector, and the NT for the Indian sector in March ( $p<0.05$ ).

428 In summary, while the magnitude of trends differs between both algorithms, there is general  
429 spatial consistency in the patterns of positive and negative trends in the consolidated pack ice  
430 and the MIZ. Results suggest that positive trends in total SIE are generally a result of  
431 statistically significant positive trends in the consolidated pack ice in the BT algorithm in all  
432 sectors of the Antarctic, except for the Bellingshausen/Amundsen Sea sector and the Weddell  
433 Sea during ice retreat. The NT algorithm on the other hand suggests more instances of  
434 statistically significant positive trends in the MIZ, though this is highly regionally dependent.  
435 Finally, the largest expansion of polynya area is found in the Bellingshausen/Amundsen Sea  
436 during November, whereas small increases in polynya area are found in both the Indian and  
437 Pacific sector during the ice expansion phase. Outside of these regions/months, no significant  
438 changes in coastal polynya area are observed.

### 439 3.2.3 Seasonal Trends in MIZ and Pack Ice Width

440 Finally we compute the overall width of the MIZ and pack ice following *Strong and Rigor*  
441 [2013] and produce seasonal means. Time-series of seasonal means of the circumpolar MIZ  
442 width and pack ice width are shown in **Figure 10** for all seasons except summer when the  
443 results are noisy. As we may expect following the previous results, the NASA Team algorithm  
444 consistently shows greater MIZ width and smaller pack ice width than the Bootstrap algorithm.  
445 During autumn (MAM) however, the differences between the algorithms are reduced, both for  
446 the MIZ and pack ice widths. In addition, during this season, trends in the MIZ and pack ice are  
447 largely consistent, with no trend in the MIZ and increases in the pack ice on the order of  $21.2 \text{ km}$   
448  $\text{dec}^{-1}$  and  $20.0 \text{ km dec}^{-1}$  ( $p<0.01$ ) for the BT and NT algorithms, respectively.

449 During winter (JJA) and spring (SON) however, the NT and BT algorithms exhibit opposing  
450 trends in the MIZ with the NT algorithm indicating an increase and the BT a decrease. The  
451 largest positive trend in the MIZ width occurs during spring at a rate of  $+10.3 \text{ km dec}^{-1}$  ( $p<0.01$ )  
452 in the NT algorithm, indicating a 6% widening over the satellite record. This widening is a result  
453 of the MIZ moving slightly equatorward rather than expanding southwards. However, despite a



454 statistically significant trend, there remains substantial interannual variability in the SON MIZ  
455 width, with the maximum width recorded in 2003 (310 km) and the minimum in 1985 (217 km),  
456 with a mean SON MIZ width of 248 km. The trend during winter is considerably smaller at +2.7  
457 km dec<sup>-1</sup>, as a result of expansion equatorward and southwards, yet it is not statistically  
458 significant.

459 For the pack ice, both algorithms show statistically significant positive trends towards  
460 increased width of the pack ice, which are also nearly identical during winter at +18.7 and +18.1  
461 km dec<sup>-1</sup> ( $p < 0.01$ ) for the BT and NT algorithms, respectively. This represents a widening of the  
462 pack ice of approximately 11% from 1979 to 2014 during winter. As one may expect, differences  
463 in the pack ice width between the algorithms are largely found in spring as a result of the MIZ  
464 expanding in the NT algorithm. During SON the trends in the width of the pack ice are slightly  
465 smaller than during winter, with trends of +16.7 (BT,  $p < 0.01$ ) and +10.0 (NT,  $p < 0.05$ ) km dec<sup>-1</sup>.

466 Interestingly, the interannual variability in the pack ice is similar between both data sets,  
467 showing correlations between the two algorithms of 0.92 (JJA), 0.77 (SON) and 0.96 (MAM).  
468 For the MIZ, interannual variability is generally about twice as large in the NASA Team  
469 algorithm and the two data sets are not highly correlated except for autumn, with correlations of  
470 0.39 (JJA), 0.43 (SON), and 0.67 (MAM).

#### 471 **4. Implications for a Seabird**

472 Here we use data on the MIZ and the consolidated ice pack from both algorithms to  
473 understand the role of sea ice habitat on breeding success of a seabird, the snow petrel  
474 *Pagodroma nivea*. As mentioned in the introduction, the MIZ is a biologically important region  
475 because it is an area of high productivity and provides access to food resources needed by  
476 seabirds [Ainley *et al.*, 1992]. During winter, productivity is reduced at the surface in open water,  
477 while it is concentrated within the ice habitat, especially within the ice floes [Ainley *et al.*, 1986].  
478 This patchy distribution of food availability within the MIZ and pack ice provides feeding  
479 opportunities for seabirds such as the snow petrel. Observations suggest that the snow petrel  
480 forages more successfully in areas close to the ice edge and within the MIZ than in consolidated  
481 ice conditions [Ainley *et al.*, 1984, 1992].

482 Breeding success of snow petrels depends on sufficient body condition of the females,  
483 which in part reflects favorable environmental and foraging conditions prior to the breeding  
484 season. Indeed, female snow petrels in poor early body condition are not able to build up the  
485 necessary body reserves for successful breeding [Barbraud and Chastel, 1999]. Breeding  
486 success was found to be higher during years with extensive sea ice cover during the preceding  
487 winter [Barbraud and Weimerskirch, 2001]. This is in part because winters with extensive sea  
488 ice are associated with higher krill abundance the following summer [Flores *et al.*, 2012; Loeb  
489 *et al.*, 1993; Atkinson *et al.*, 2004], thereby increasing the resource availability during the breeding  
490 season. However, extensive winter sea ice may protect the under ice community from predation  
491 and thus reduce food availability, in turn affecting breeding success [Olivier *et al.*, 2005]. By  
492 distinguishing between the areas of MIZ and pack ice, we can expect a better understanding of  
493 the role of sea ice on food availability and hence breeding success of snow petrels.



494 In the following, we expect that an extensive pack ice may reduce breeding success by  
495 protecting the under ice community from predation, while an extensive MIZ may increase  
496 breeding success by providing easier access to foraging. With the classifications as defined by  
497 both algorithms we calculated the MIZ and pack ice area in a wide rectangular sector defined by  
498 the migration route of the snow petrel [Delord *et al.*, 2013] from April to September [see **Table 4**  
499 for latitude and longitude limits]. We then averaged the MIZ and pack ice extents over the entire  
500 winter from April to September. We next employed a logistic regression approach to study the  
501 effects of MIZ and pack ice area within this sector and evaluate the impacts on breeding  
502 success the following summer. The response variable was the number of chicks  $C_t$  in a breeding  
503 season  $t$ , from 1979 to 2014 collected at Terre Adélie, Dumont D'Urville [Barbraud and  
504 Weimerskirch, 2001, Jenouvrier *et al.*, 2005].

505 Effects of MIZ and pack ice area were analyzed using Generalized Linear Models (GLM)  
506 with logit-link functions and binomial errors fitted in R using the package glm. We selected the  
507 best model according to the information criteria AIC, the chosen model being the one that  
508 minimizes the AIC, and the ability of two models to describe the data was assumed to be “not  
509 different” if the difference in their AIC was  $< 2$  [Burnham and Anderson, 2002]. While non-linear  
510 models may be more appropriate as ecological system relationships are likely more complex  
511 than linear relationships, without *a priori* knowledge of the mechanisms that could lead to such  
512 non-linear relationships, it is extremely difficult to interpret the results.

513 **Table 5** summarizes model selection. The model with the lowest AIC suggests an effect of  
514 the consolidated pack ice area on breeding success as derived from the Bootstrap algorithm.  
515 The MIZ and pack ice areas calculated from the NT algorithm are not supported (AIC  
516 difference  $> 2$ ). As expected we found that the effect of consolidated pack ice on breeding  
517 success was negative [**Figure 11**]. In other words, more extensive consolidated pack ice during  
518 winter tends to reduce breeding success the following summer by limiting foraging opportunities.  
519 The effect of the MIZ however was uncertain, contrary to what one may expect given the  
520 increased opportunities for foraging within the MIZ. However, if we had only used ice  
521 classifications based on the NASA Team algorithm, the model with the lowest AIC would have  
522 suggested an importance of the MIZ. We would have then concluded a negative effect of the  
523 MIZ on the breeding success of snow petrels, contrary to what one may expect given that the  
524 MIZ is the main feeding habitat of the species. By using both algorithms, we instead conclude  
525 that the breeding success of snow petrels is negatively affected by the pack ice area as  
526 calculated with the Bootstrap algorithm.

## 527 **5. Discussion**

528 The positive trends in Antarctic sea ice extent are currently poorly understood and are at  
529 odds with climate model forecasts that suggest the sea ice should be declining in response to  
530 increasing greenhouse gases and stratospheric ozone depletion [e.g. Turner *et al.*, 2013; Bitz  
531 and Polvani, 2012; Sigmond and Fyfe, 2010]. However, several modeling studies, such as those  
532 used in the phase 5 Coupled Model Intercomparison Project (CMIP5), have suggested that the  
533 sea ice increase over the last 36 years remains within the range of intrinsic of internal variability  
534 [e.g. Bitz and Polvani, 2012; Turner *et al.*, 2013; Mahlstein *et al.*, 2013; Polvani and Smith,



535 2013; *Swart and Fyfe*, 2013]. Earlier satellite from the 1960s and 1970s and from ship  
536 observations suggest periods of high and low sea ice extent, and thus high natural variability  
537 [*Meier et al.*, 2013; *Gallaher et al.*, 2014]. Further evidence comes from ice core climate records,  
538 which suggest that the climate variability observed in the Antarctic during the last 50 years  
539 remains within the range of natural variability seen over the last several hundred to thousands of  
540 years [*Thomas et al.*, 2013; *Steig et al.*, 2013]. Thus, we may require much longer records to  
541 properly assess Antarctic sea ice trends in contrast to the Arctic, where negative trends are  
542 outside the range of natural variability and are consistent with those simulated from climate  
543 models.

544 While many assessments of how Antarctic sea ice trends and variability compare with  
545 climate models have focused on the net circumpolar sea ice extent, it is the regional variability  
546 that becomes more important. For example, *Hobbs et al.* [2015] argue that when viewing trends  
547 on a regional basis, the observed summer and autumn trends fall outside of the range of natural  
548 variability as simulated by present-day climate models, with the signal dominated by opposing  
549 trends in the Ross Sea and the Bellingshausen/Amundsen seas. These results have questioned  
550 the ability of climate models to correctly simulate processes at the regional level and within the  
551 southern ocean-atmosphere-sea ice coupled system.

552 The net take-away point from these studies is that the net circumpolar changes in sea ice  
553 extent do not enhance our understanding of how the Antarctic sea ice is changing. Instead our  
554 focus should be on what drives regional and seasonal sea ice changes, including feedbacks  
555 and competing mechanisms. This study aims to better understand regional and total changes in  
556 Antarctic sea ice by focusing not only on the total ice area, but also on how the consolidated  
557 pack ice, the marginal ice zone and coastal polynyas are changing. Differences in climatologies  
558 and trends of the different ice classes may suggest different processes are likely contributing to  
559 their seasonal and interannual variability. In addition, the different contributions of ice types  
560 towards the overall expansion of the Antarctic sea ice cover between algorithms may in turn  
561 influence attribution of the observed increase in SIE. For example, within the highly dynamic  
562 MIZ region, intense atmosphere-ice-ocean interactions take place [e.g. *Lubin and Massom*,  
563 2006] and thus an expanding or shrinking MIZ may help to shed light on the relative importance  
564 of atmospheric or oceanic processes impacting the observed trends in total SIE. Another issue  
565 is whether or not new ice is forming along the outer edge of the pack ice or if it is all being  
566 dynamically transported from the interior.

567 However, a complication exists, what sea ice algorithm should be used for such  
568 assessments? In this study we focused on using passive microwave satellite data for defining  
569 the different ice types as it is the longest time-series available and is not limited by polar  
570 darkness or clouds. However, results may be highly dependent on which sea ice algorithm is  
571 used to look at the variability in these ice classes, which will also be important in assessing  
572 processes contributing to these changes as well as implications of these changes to the polar  
573 marine ecosystem. In this study, the positive trends in circumpolar sea ice extent over the  
574 satellite data record are primarily driven by statistically significant trends ( $p < 0.05$ ) in expansion  
575 of the consolidated pack ice in both sea ice algorithms. However, an exception occurs in the  
576 NASA Team sea ice algorithm after the ice pack reaches its seasonal maximum extent when



577 the positive trends in the pack ice are no longer as large, nor statistically significant. Instead,  
578 positive trends in the MIZ dominate during September and October ( $p < 0.10$ ). This is in stark  
579 contrast to the Bootstrap algorithm, which shows a declining MIZ area from March through  
580 November.

581 The algorithms also give different proportions of how much the total ice cover consists of  
582 consolidated ice, MIZ or polynya area. In some regions, such as the Pacific Ocean sector, the  
583 NT algorithm suggests the MIZ is the dominant ice type whereas in the BT algorithm, the pack  
584 ice is dominant, which is true for all sectors analyzed in the Bootstrap algorithm. Considering the  
585 circumpolar ice cover, the MIZ in the NASA Team algorithm is on average twice as large as in  
586 the Bootstrap algorithm. In the Arctic, *Strong and Rigor* [2013] found the NASA Team algorithm  
587 gave about three times wider MIZ than the Bootstrap algorithm. In this case, the Bootstrap  
588 results agreed more with MIZ widths obtained from the National Ice Center (NIC).

589 Differences between the algorithms are not entirely surprising as the two algorithms use  
590 different channel combinations with different sensitivities to changes in physical temperature. In  
591 addition, the NT uses previously defined tie points for passive microwave radiances over known  
592 ice-free ocean, and ice types, defined as type A and B in the Antarctic, as the radiometric  
593 signature between first-year and multiyear ice in the Antarctic is lost. The ice is assumed to be  
594 snow-covered when selecting the tie points, which can result in an underestimation of sea ice  
595 concentration if the ice is not snow covered. In addition, seasonal variations in sea ice emissivity  
596 can be very large, leading to seasonal biases in either algorithm. The advantage of the  
597 Bootstrap algorithm is that the ice concentration can be derived without an *a priori* assumption  
598 about ice type, though consolidated ice data points are sometimes difficult to distinguish from  
599 mixtures of ice and open ocean due to the presence of snow cover, flooding or roughness  
600 effects.

601 While one may expect the Bootstrap algorithm to provide more accurate results than the  
602 NASA Team algorithm, near the coast the BT algorithm has been shown to have difficulties  
603 when temperatures are very cold. Because the NT algorithm uses brightness temperature ratios  
604 it is largely temperature independent. However, during summer or for warmer temperatures, the  
605 NT algorithm may indeed be biased towards lower sea ice concentrations whereas the BT  
606 algorithm may be biased towards higher ice concentrations [e.g. *Comiso et al.*, 1997]. In the  
607 Arctic, the MIZ is not only driven by wave mechanics and flow breaking (dynamic origin), but  
608 also by melt pond processes in summer (thermodynamic origin) [*Arnsten et al.*, 2015]. Thus,  
609 larger sensitivity of the NT algorithm to melt processes may be one reason for the large  
610 discrepancy observed in the Arctic. Interestingly, the BT algorithm shows less interannual  
611 variability in the ice types compared to NT (as shown by the smaller standard deviations). This  
612 would in turn influence assessments of atmospheric or oceanic conditions driving observed  
613 changes in the ice cover. What is clear is that more validation is needed to assess the accuracy  
614 of these data products, especially for discriminating the consolidated pack ice from the MIZ.  
615 Errors likely are larger in the MIZ because of the coarse spatial resolution of the satellite  
616 sensors. Another concern is that mapping of the consolidated ice pack does not always mean a  
617 compact ice cover. The algorithms may indicate 100% sea ice concentration (e.g. a



618 consolidated pack ice), when in reality the ice consists of mostly brash ice and small ice floes  
619 more representative of the MIZ. Future work will focus on validation with visible imagery.

## 620 Conclusions

621 Total Antarctic sea ice cover is expanding in response to atmospheric and oceanic variability  
622 that remains to be fully understood. One may expect that these increases would also be  
623 manifested in either equatorward progression of the MIZ or the consolidated pack ice or both. In  
624 this study we identified several different ice categories using two different sets of passive  
625 microwave sea ice concentration data sets. The algorithms are in agreement as to the location  
626 of the northern edge of the total sea ice cover, but differ in regards to how much of the ice cover  
627 consists of the marginal ice zone, the consolidated ice pack, the size of potential polynyas as  
628 well as the amount of broken ice and open water within the consolidated ice pack. Here we use  
629 sea ice concentration thresholds of  $0.15 \leq \text{SIC} < 0.80$  to define the width of the MIZ and  $0.80 \leq$   
630  $\text{SIC} \leq 1.0$  to define the consolidated pack ice. Yet applying the same thresholds for both sea ice  
631 algorithms results in a MIZ from the NASA Team algorithm that is on average twice as large as  
632 in the Bootstrap algorithm and considerably more broken ice within the consolidated pack ice.  
633 Total potential coastal polynya areas ( $\text{SIC} \leq 0.80$ ) also differ between the algorithms, though  
634 differences are generally smaller than for the other ice types analyzed.

635 While the spatial extents of the different ice classes may differ, the seasonal cycle is  
636 generally consistent between both algorithms. Climatologically, the advance of the consolidated  
637 ice pack happens over a much longer period (~7-8 months) than the retreat (~4-5 months),  
638 while the MIZ exhibits a longer advance period (~8-10 months). This seasonal cycle in  
639 expansion/contraction of the ice cover is in general agreement with results by *Stammerjohn et*  
640 *al.* [2008] who showed sea ice retreat generally begins in September at the outer most edge of  
641 the sea ice and continues poleward over the next several months. However, what these results  
642 show is that while the pack ice starts to retreat around September, this in turn results in a further  
643 expansion of the MIZ, the amount of which is highly dependent on which algorithm is used. The  
644 timing of when the maximum polynya extent is reached however can differ by several months  
645 between the algorithms in regions such as the Bellingshausen/Amundsen Sea and the Pacific  
646 Ocean.

647 Since the MIZ is an important region for phytoplankton biomass and productivity [e.g. *Park*  
648 *et al.*, 1999], mapping seasonal and interannual changes in the MIZ is important for  
649 understanding changes in top predator populations and distributions. However, as mentioned  
650 above, results are highly dependent on which sea ice algorithm is used for delineating the MIZ.  
651 Furthermore, accurately mapping the extent of the MIZ from coarse resolution satellite data  
652 such as that from passive microwave sensors remains problematic. The MIZ is very dynamic in  
653 space and time, making it challenging to provide precise delimitations using sea ice  
654 concentrations that are in turn sensitive to melt processes and surface conditions. Nevertheless  
655 we examined the impact the winter MIZ and consolidated pack ice area as derived from both  
656 algorithms would have on the breeding success of snow petrels the following summer. The  
657 different proportions of MIZ and consolidated pack ice between algorithms affected the  
658 inferences made from models tested even if trends were of the same sign. Given the sensitivity





659 of the relationships between ice types and breeding success of this species, caution is  
660 warranted when doing this type of analysis as different relationships may emerge as a function  
661 of which sea ice data set is used in the analysis. Further work is needed to validate the  
662 accuracy of the ice types from passive microwave.

### 663 **Acknowledgements**

664 This work is funded under NASA Grant NNX14AH74G and NSF Grant PLR 1341548. We are grateful to  
665 Sharon Stammerjohn for her helpful comments on the manuscript. Gridded fields of the different ice  
666 classifications from both algorithms are available via ftp by contacting J. Stroeve. We thank all the  
667 wintering fieldworkers involved in the collection of snow petrel data at Dumont d'Urville since more  
668 than 50 years, as well as Institut Paul Emile Victor (program IPEV n°109, resp. H. Weimerskirch), Terres  
669 Australes et Antarctiques Françaises and Zone Atelier Antarctique (CNRS-INEE) for support.



## 670 References

- 671 Ainley, D.G., E. O'Connor, and R.J. Boekelheide. (1984). The marine ecology of birds in the  
672 Ross Sea, Antarctica, *Ornithological Monographs*, 32, 1-97.
- 673 Ainley, D. G., W.R. Fraser, C.W. Sullivan, J.J. Torres and T.L. Hopkins et al. (1986), Antarctic  
674 mesopelagic micronekton: Evidence from seabirds that pack ice affects community structure,  
675 *Science*, 232:847-849.
- 676 Ainley, D.G., Ribic, C. A., and Fraser, W. R. (1992). Does prey preference affect habitat choice  
677 in Antarctic seabirds? *Marine Ecology-Progress Series*, 90:207-221.
- 678 Ainley, D., J. Russell, S. Jenouvrier, E. Woehler, P. O. B. Lyver, W. R. Fraser, and G. L.  
679 Kooyman (2010), Antarctic penguin response to habitat change as Earth's troposphere reaches  
680 2 C above preindustrial levels, *Ecological Monographs*, 80(1), 49-66.
- 681 Arnsten, A.E., A.J. Song, D.K. Perovich and J.A. Richter-Menge, (2015), Observations of the  
682 summer breakup of an Arctic sea ice cover, *Geophys. Res. Lett.*, doi:10.1002/1015GL065224.
- 683 Arrigo, K. R., and G. L. van Dijken (2003), Phytoplankton dynamics within 37 Antarctic coastal  
684 polynya systems, *Journal of Geophysical Research: Oceans (1978–2012)*, 108(C8).
- 685 Arrigo, K., G. L. van Dijken, and A. Strong (2015), Environmental controls of marine  
686 productivity hot spots around Antarctica, *J. Geophys. Res.-Oceans*,  
687 doi:10.1002/2015JC010888.
- 688 Atkinson, A., Siegel, V., Pakhomov, E., & Rothery, P. (2004). Long-term decline in krill stock  
689 and increase in salps within the Southern Ocean. *Nature*, doi:10.1038/nature02996.
- 690 Barbraud C., and O. Chastel, (1999), Early body condition and hatching success in the snow  
691 petrel *Pagodroma nivea*. *Polar Biol.*, 21:1-4.
- 692 Barbraud C. and H. Weimerskirch (2001), Contrasting effects of the extent of sea-ice on the  
693 breeding performance of an Antarctic top predator, the snow petrel *Pagodroma nivea*. *J. Avian*  
694 *Biol.*, 32:297-302
- 695 Bintanja, R., G. J. Van Oldenborgh, S. S. Drijfhout, B. Wouters, and C. A. Katsman, (2013),  
696 Important role for ocean warming and increased ice-shelf melt in Antarctic sea-ice expansion,  
697 *Nat. Geosci.*, 6, 376–379, doi:10.1038/ngeo1767.
- 698 Bitz, C.M. and L.M. Polvani, (2012), Antarctic climate response to stratospheric ozone depletion  
699 in a fine resolution ocean climate model, *Geophys. Res. Lett.*, doi:10.1029/2012GL053393.
- 700 Boyd PW, Jickells T, Law CS, Blain S, Boyle EA, et al. (2007). Mesoscale iron enrichment  
701 experiments 1993–2005: Synthesis and future directions. *Science* **315**: 612–617
- 702 Burnham, K. P., and D. R. Anderson. 2002. Model selection and multimodel inference : a  
703 practical information-theoretic approach. Springer, New York.
- 704 Cavalieri, D. J., C. L. Parkinson, P. Gloersen, J. C. Comiso, and H. J. Zwally, (1999), Deriving  
705 Long-Term Time Series of Sea Ice Cover from Satellite Passive-Microwave Multisensor Data  
706 Sets, *J. Geophys. Res.*, 104, 15,803-15,814.
- 707 Chiswell, S. M. (2011), Annual cycles and spring blooms in phytoplankton: don't abandon  
708 Sverdrup completely, *Marine Ecology Progress Series*, 443, 39-50.
- 709 Comiso, J. C., and F. Nishio. 2008. Trends in the Sea Ice Cover Using Enhanced and Compatible  
710 AMSR-E, SSM/I, and SMMR Data. *J. Geophys. Res.*, 113, C02S07,  
711 doi:10.1029/2007JC0043257.
- 712 Comiso, J. C., D. Cavalieri, C. Parkinson, and P. Gloersen. 1997. Passive Microwave Algorithms  
713 for Sea Ice Concentrations: A Comparison of Two Techniques. *Rem. Sens. Environ.*,  
714 60(3):357-84.



- 715 Delord, K., C. Barbraud, C.A. Bost, Y. Cherel, C. Guinet, and H. Weimerskirch. 2013. Atlas of  
716 top predators from French Southern Territories in the Southern Indian Ocean. CEBC-CNRS.  
717 pp. 252.
- 718 Ferrari, R., S. T. Merrifield, and J. R. Taylor (2014), Shutdown of convection triggers increase of  
719 surface chlorophyll, *J. Marine Systems*, doi:10.1016/j.jmarsys.2014.02.009.
- 720 Flores, H., J. Andries van Franeker, V. Siegel, M. Haraldsson, V. Strass, E.H. Meesters, U.  
721 Bathmann, and W.-J. Wolff, (2012), The Association of Antarctic Krill *Euphausia superba*  
722 with the Under-Ice Habitat, *Plos One*, doi:10.1371/journal.pone.0031775.
- 723 Fogt RL, Wovrosh AJ, Langen RA, Simmonds I (2012) The characteristic variability and  
724 connection to the underlying synoptic activity of the Amundsen–Bellingshausen Seas low, *J*  
725 *Geophys Res.* doi:10.1029/2011JD017337
- 726 Gallaher, D., G. G. Campbell, and W. N. Meier (2014), Anomalous variability in Antarctic sea  
727 ice extents during the 1960s with the use of Nimbus data. *IEEE J. Selected Topics in Appl.*  
728 *Earth Obs. And Rem. Sens.*, 7(3), 881-887, doi:10.1109/JSTARS.2013.2264391.
- 729 Gloersen, P., W. J. Campbell, D. J. Cavalieri, J. C. Comiso, C. L. Parkinson, H. J. Zwally,  
730 "Arctic and Antarctic Sea Ice, 1978-1987L Satellite Passive Microwave Observations and  
731 Analysis," *NASA Spec. Publ.*, Vol. 511, 290 pp, 1992.
- 732 Hobbs, W.R. and M.N. Raphael (2010), The Pacific zonal asymmetry and its influence on  
733 Southern Hemisphere sea ice variability. *Antarctic Science*, 22 (05), 559-571, doi:  
734 10.1017/S0954102010000283.
- 735 Hosking JS, Orr A, Marshall GJ, Turner J, Phillips T (2013) The influence of the Amundsen–  
736 Bellingshausen Seas low on the climate of West Antarctica and its representation in coupled  
737 climate model simulations. *J Clim.*, 26:6633–6648
- 738 Ivanova, N., and others, (2015), Satellite passive microwave measurements of sea ice  
739 concentration: an optimal algorithm and challenges, *The Cryosphere Discuss.*, 9,  
740 doi:10.5194/tcd-9-1269-2015.
- 741 Ivanova, N., O.M. Johannessen, L. Toudal Pederson and R.T. Tomboe (2014), Retrieval of  
742 Arctic sea ice parameters by satellite passive microwave sensors: A comparison of eleven sea  
743 ice concentration algorithms, *IEEE Trans. Geos. Rem. Sens.*, 52(11),  
744 doi:10.1109/TGRS.2014.2301136.
- 745 Jaiser, R., K. Dethloff, D. Handor, A. Rinke and J. Cohen, (2012), Impact of sea ice cover  
746 changes on the Northern Hemisphere atmospheric winter circulation, *Tellus*, 64, 11595,  
747 doi:10.3402/tellusa.v64i0.11595.
- 748 Jenouvrier, S., C Barbraud, and H. Weimerskirch, (2005), Long-Term Contrasted Responses to  
749 climate of two Antarctic seabird species, *Ecology* 86:2889–2903.  
750 <http://dx.doi.org/10.1890/05-0514>
- 751 Kohout, A. L., and M. H. Meylan (2008), An elastic plate model for wave attenuation and ice  
752 floe breaking in the marginal ice zone, *J. Geophys. Res.*, 113, C09016,  
753 doi:10.1029/2007JC004434.
- 754 Loeb, V. J., V. Siegel, O. Holm-Hansen, R. Hewitt, W. Fraser, W. Trivelpiece, and S. G.  
755 Trivelpiece, (1997), Effects of sea- ice extent and krill or salp dominance on the Antarctic  
756 food web, *Nature* 387:897–900.
- 757 Louzao, M., Pinaud, D., Peron, C., Delord, K., Wiegand, T., & Weimerskirch, H. (2011),  
758 Conserving pelagic habitats: seascape modelling of an oceanic top predator. *Journal of*  
759 *Applied Ecology*, 48(1), 121–132. <http://doi.org/10.1111/j.1365-2664.2010.01910.x>.



- 760 Lubin, D. and R. Massom (2006), Sea ice. In Polar remote sensing volume i: atmosphere and  
761 oceans, Springer, Berlin, pp 309-728.
- 762 Mahlstein, I. P.R. Gent and S. Solomon, (2013), Historical Antarctic mean sea ice area, sea ice  
763 trends, and winds in CMIP5 simulations, *J. Geophys. Res. Atmos.*, doi:10.1002/jgrd.50443.
- 764 Maksym, T.E. E. Stammerjohn, S. Ackley and R. Massom (2012), Antarctic sea ice – A polar  
765 opposite? *Oceanography*, 25, 140-151, doi:10.5670/oceanog.2012.88.
- 766 Meier, W., D. Gallaher, and G. G. Campbell (2013), New estimates of Arctic and Antarctic sea  
767 ice extent during September 1964 from recovered Nimbus I satellite imagery, *The Cryosphere*  
768 7, 699-705, doi:10.5194/tc-7-699-2013.
- 769 Olivier, F., Franeker, J. A. V., Creuwels, J. C. S., & Woehler, E. J. (2005), Variations of snow  
770 petrel breeding success in relation to sea-ice extent: detecting local response to large-scale  
771 processes? *Polar Biology*, 28(9), 687–699. <http://doi.org/10.1007/s00300-005-0734-5>
- 772 Park, M. K., S.R. Yang, S.H. Kang, K.H. Chung, and J.H. Shim, (1999), Phytoplankton biomass  
773 and primary production in the marginal ice zone of the northwestern Weddell Sea during  
774 austral summer, *Polar Biol.*, 21, 251–261.
- 775 Parkinson, C. L. and D.J. Cavalieri, (2012). Antarctic Sea Ice Variability and Trends, 1979–  
776 2010. *The Cryosphere*, 6:871-880. doi:10.5194/tcd-6-931-2012.
- 777 Piatt, I., & Sydeman, W. (2007), Seabirds as indicators of marine ecosystems. *Marine Ecology*  
778 *Progress Series*, 352, 199–204. <http://doi.org/10.3354/meps07070>.
- 779 Raphael, M.N. and W. Hobbs (2014), The influence of the large-scale atmospheric circulation on  
780 Antarctic sea ice during ice advance and retreat seasons, *Geophys. Res. Lett.*,  
781 doi:10.1002/2014GL060365.
- 782 Rayner, N.A., D.E. Parker, E.B. Horton, C.K. Folland, L.V. Alexander, D.P. Rowell, E.C. Kent,  
783 and A. Kaplan, (2003), Global analyses of sea surface temperature, sea ice, and night marine  
784 air temperature since the late nineteenth century, *J. Geophys. Res.*, 118,  
785 doi:10.1029/2002JD002670.
- 786 Reid, P., S. Stammerjohn, R. Massom, T. Scambos, and J. Leiser (2015), The record 2013  
787 Southern Hemisphere sea-ice extent maximum. *Ann. Glaciology*, 56(69), pp. 99-106(8).
- 788 Serreze, M.C. and J.C. Stroeve, (2015), Arctic Sea Ice Trends, Variability and Implications for  
789 Seasonal Ice Forecasting, *Phil. Trans. A.*, 373, 20140159, doi:10.1098/rsta.2014.0159.
- 790 Smith Jr, W. O., and D. Barber (2007), *Polynyas: Windows to the World: Windows to the World*,  
791 Elsevier.
- 792 Stammerjohn, S.E., D.G. Martinson, R.C. Smith, X. Yuan and D. Rind, (2008), Trends in  
793 Antarctic annual sea ice retreat and advance and their relation to El Nino-Southern Oscillation  
794 and Southern Annular Mode variability, *J. Geophys. Res.*, 108, C03S90,  
795 doi:10.1029/2007JC004269.
- 796 Stammerjohn, S., R. Massom, D. Rind, and D. Martinson, 2012: Regions of rapid sea ice change:  
797 An inter-hemispheric seasonal comparison. *Geophys. Res. Lett.*, 39, L06501,  
798 doi:10.1029/2012GL050874.
- 799 Sigmond, M. and J.C. Fyfe, (2010), Has the ozone hole contributed to increased Antarctic sea ice  
800 extent?, *Geophys. Res. Lett.*, 37, L18502, doi:10.1029/2010GL044301.
- 801 Steig, E. J., et al. (2013), Recent climate and ice-sheet changes in West Antarctica compared  
802 with the past 2,000 years, *Nat. Geosci.*, 6, 372–375.
- 803 Stroeve, J.C., M.C. Serreze, J.E. Kay, M.M. Holland, W.N. Meier and A.P. Barrett (2012), The  
804 Arctic's rapidly shrinking sea ice cover: A research synthesis, *Clim. Change*, doi:  
805 10.1007/s10584-011-0101-1.



- 806 Strong, C. and I.G. Rigor, (2013), Arctic marginal ice zone trending wider in summer and  
807 narrower in winter, *Geophys. Res. Lett.*, 40, doi:10.1002/grl.50928.
- 808 Swart, N.C. and J.C. Fyfe, (2013), The influence of recent Antarctic ice sheet retreat on  
809 simulated sea ice area trends, *Geophys. Res. Lett.*, doi:1002/grl.50820.
- 810 Thomas, E.R., T.J. Bracegirdle, J. Turner and E.W. Wolff, (2013), A 308 year record of climate  
811 variability in West Antarctica, *Geophys. Res. Lett.*, doi:10.1002/2013GL057782.
- 812 Turner J, T. Phillips, S. Hosking, G.T. Marshall and A. Orr, (2012) The Amundsen Sea Low, *Int*  
813 *J. Climatol.*, 33:1818–1829.
- 814 Turner J., J. S. Hosking, T. Phillips, and G. J. Marshall, (2013), Temporal and spatial evolution  
815 of the Antarctic sea ice prior to the September 2012 record maximum extent. *Geophys. Res.*  
816 *Lett.*, 40, 5894–5898, doi: 10.1002/2013GL058371.
- 817 Turner, J., J.S. Hosking, G.J. Marshall, T. Phillips, T.J. Bracegirdle, (2015), Antarctic sea ice  
818 increase consistent with intrinsic variability of the Amundsen Sea Low, *Clim. Dyn.*,  
819 doi:10.1007/s00382-015-2709-9.
- 820 Wadhams, P., (1986), The seasonal ice zone, The Geophysics of Sea Ice, NATO ASI  
821 Series, 825–991, 1986. DOI:10.1007/978-1-4899-5352-0\_15.
- 822 Wang, X. L., Y. Feng, V.R. Swail and A. Cox, (2015), Historical changes in the Beaufort-  
823 Chukchi-Bering seas surface winds and waves, 1971-2013, *J. Climate*, doi:10.1175/JCLI-D-  
824 15-0190.1
- 825 Watkins, A.B. and I. Simmonds, (1999), A late spring surge in open water of the Antarctic sea  
826 ice pack, *Geophys. Res. Lett.*, 26, doi:10.1029/1999GL900292.
- 827 Yun, L., R. Ji, S. Jenouvrier, M. Jin and J. Stroeve, (2015), Synchronicity between ice retreat and  
828 phytoplankton bloom in circum-Antarctic Polynyas, submitted to Geophysical Research  
829 Letters, in revision.
- 830



831 **Tables**

832 **Table 1.** Sea ice categories defined in this study.

Region	Definition	Binary Classification Value
Outer MIZ	Outer region of sea ice with ice concentration between 15% and 80%	16
Inner Polynya	Region near the coast with concentration < 80% south of 80% concentration	32
Distant ice	Scattered sea ice regions north of MIZ, possibly islands or atmospheric storms	48
Pack Ice	Ice concentration > 80%	80
Inner open water	Concentration < 15% south of MIZ	112
Open pack ice	Concentration > 15% and < 80% within consolidated ice region	128

833

834



835 **Table 2.** Monthly mean extents of the different ice classes. Values are only listed for the consolidated  
 836 pack ice, the marginal ice zone and the potential coastal polynya area. Values are listed in  $10^6$  km<sup>2</sup>.

	NASA Team			Bootstrap		
	Total Antarctic					
Month	MIZ	Polynya	Pack Ice	MIZ	Polynya	Pack Ice
January	2.44	0.31	1.94	2.06	0.36	2.27
February	1.51	0.20	1.18	1.25	0.22	1.49
March	2.03	0.25	1.42	1.65	0.24	2.08
April	2.71	0.42	3.27	1.84	0.31	4.62
May	3.07	0.62	5.85	1.97	0.37	7.79
June	3.63	0.69	8.22	2.31	0.37	10.65
July	4.03	0.66	10.31	2.53	0.35	13.00
August	4.75	0.62	11.29	2.88	0.34	14.49
September	5.41	0.63	11.31	3.19	0.35	14.89
October	5.41	0.74	10.83	3.39	0.38	14.16
November	5.62	1.02	7.92	3.69	0.63	11.10
December	5.05	0.88	3.81	3.56	0.81	5.43
Annual	3.83	0.59	6.49	2.54	0.39	8.53
	Ross Sea					
Month	MIZ	Polynya	Pack Ice	MIZ	Polynya	Pack Ice
January	0.83	0.10	0.28	0.68	0.13	0.40
February	0.47	0.05	0.11	0.40	0.07	0.19
March	0.62	0.10	0.34	0.45	0.09	0.57
April	0.60	0.15	1.22	0.37	0.09	1.63
May	0.60	0.15	1.93	0.36	0.08	2.43
June	0.67	0.15	2.29	0.40	0.08	2.91
July	0.75	0.14	2.63	0.44	0.07	3.27
August	0.91	0.12	2.67	0.50	0.07	3.43
September	0.98	0.13	2.64	0.54	0.08	3.46
October	0.86	0.17	2.73	0.55	0.09	3.39
November	0.89	0.30	2.19	0.59	0.17	2.87
December	1.17	0.32	0.92	0.76	0.26	1.45
Annual	0.78	0.16	1.67	0.50	0.11	2.18
	Bellinghausen/Amundsen Sea					
Month	MIZ	Polynya	Pack Ice	MIZ	Polynya	Pack Ice
January	0.35	0.07	0.32	0.29	0.08	0.38
February	0.28	0.05	0.16	0.22	0.06	0.21
March	0.37	0.06	0.10	0.27	0.07	0.21
April	0.50	0.07	0.20	0.29	0.06	0.48
May	0.54	0.12	0.42	0.31	0.06	0.83
June	0.63	0.16	0.66	0.37	0.05	1.17
July	0.68	0.17	0.89	0.43	0.05	1.45
August	0.79	0.15	1.01	0.51	0.05	1.60
September	0.84	0.14	1.00	0.51	0.05	1.62
October	0.73	0.14	0.97	0.46	0.06	1.50
November	0.69	0.13	0.86	0.45	0.08	1.25
December	0.57	0.11	0.55	0.42	0.11	0.72
Annual	0.58	0.12	0.60	0.38	0.06	0.96
	Weddell Sea					
Month	MIZ	Polynya	Pack Ice	MIZ	Polynya	Pack Ice
January	0.72	0.12	0.93	0.60	0.11	1.07
February	0.37	0.08	0.70	0.30	0.06	0.84
March	0.47	0.06	0.87	0.38	0.04	1.07
April	0.69	0.07	1.49	0.46	0.05	1.87
May	0.82	0.10	2.53	0.54	0.06	3.04
June	0.96	0.10	3.62	0.64	0.06	4.21
July	1.08	0.08	4.51	0.65	0.05	5.16



August	1.39	0.08	4.73	0.75	0.06	5.62
September	1.62	0.09	4.67	0.83	0.06	5.78
October	1.51	0.13	4.42	0.84	0.07	5.48
November	1.53	0.31	3.34	0.86	0.14	4.56
December	1.87	0.33	1.65	1.24	0.30	2.33
Annual	1.09	0.13	2.80	0.67	0.09	3.43
<b>Indian Ocean</b>						
<b>Month</b>	<b>MIZ</b>	<b>Polynya</b>	<b>Pack Ice</b>	<b>MIZ</b>	<b>Polynya</b>	<b>Pack Ice</b>
January	0.26	0.01	0.16	0.23	0.02	0.18
February	0.15	0.01	0.06	0.14	0.01	0.08
March	0.24	0.01	0.03	0.24	0.02	0.06
April	0.43	0.01	0.16	0.35	0.05	0.30
May	0.57	0.13	0.55	0.43	0.08	0.80
June	0.75	0.14	1.04	0.53	0.08	1.40
July	0.82	0.13	0.59	0.54	0.07	2.05
August	0.87	0.11	2.09	0.57	0.06	2.59
September	1.03	0.12	2.24	0.67	0.07	2.81
October	1.33	0.15	2.02	0.87	0.08	2.71
November	1.62	0.18	1.10	1.13	0.13	1.75
December	0.94	0.07	0.37	0.74	0.09	0.55
Annual	0.75	0.10	0.96	0.54	0.06	1.29
<b>Pacific Ocean</b>						
<b>Month</b>	<b>MIZ</b>	<b>Polynya</b>	<b>Pack Ice</b>	<b>MIZ</b>	<b>Polynya</b>	<b>Pack Ice</b>
January	0.28	0.01	0.24	0.25	0.02	0.26
February	0.23	0.01	0.14	0.19	0.02	0.17
March	0.34	0.02	0.10	0.31	0.03	0.15
April	0.51	0.05	0.20	0.38	0.06	0.34
May	0.54	0.11	0.43	0.35	0.10	0.67
June	0.61	0.14	0.62	0.38	0.11	0.93
July	0.70	0.14	0.73	0.45	0.10	1.10
August	0.81	0.14	0.79	0.54	0.09	1.19
September	0.93	0.14	0.76	0.63	0.10	1.17
October	0.96	0.14	0.71	0.68	0.09	1.08
November	0.88	0.10	0.44	0.66	0.11	0.70
December	0.49	0.05	0.30	0.41	0.06	0.38
Annual	0.61	0.09	0.46	0.44	0.07	0.69





838 **Table 3.** Comparison of trends in the marginal ice zone, polynyas and the consolidated pack ice for  
 839 March through November (1979 to 2013) for both the NASA Team and Bootstrap sea ice algorithms.  
 840 Trends are computed in km<sup>2</sup> per year. Statistical significance at the 90<sup>th</sup>, 95<sup>th</sup> and 99<sup>th</sup> percentiles are  
 841 denoted by <sup>+</sup>, <sup>++</sup> and <sup>+++</sup>, respectively. Results are only shown for March through November.

	NASA Team			Bootstrap		
<b>Total Antarctic</b>						
Month	dMIZ/dt	dPoly/dt	dPack/dt	dMIZ/dt	dPoly/dt	dPack/dt
March	+2,900	+700	+14,300 <sup>+++</sup>	+4,900	-300	+18,000 <sup>+++</sup>
April	-8,200	-500	+29,600 <sup>+++</sup>	-10,400	-1000	+38,000 <sup>+++</sup>
May	-9,400	-2,400	+35,000 <sup>+++</sup>	-8,500	-2,200	+41,300 <sup>+++</sup>
June	-10,100	-5,100	+32,900 <sup>+++</sup>	-9,200	-2,400	+52,400 <sup>+++</sup>
July	-3,400	-5,700	+22,600 <sup>++</sup>	-6,600	-2,300	+25,200 <sup>+++</sup>
August	+3,700	-3,600	+11,900	-6,200	-1,500	+31,800 <sup>+++</sup>
September	+10,900 <sup>+</sup>	-3,300	+3,700	-4,200	-1,400	+39,400 <sup>+++</sup>
October	+9,600 <sup>+</sup>	-4,900	+7,300	-4,300	-2,900	+25,200 <sup>+++</sup>
November	+2,600	-4,000	+6,000	-9,800	-3,700	+29,400 <sup>+++</sup>
<b>Ross Sea</b>						
Month	dMIZ/dt	dPoly/dt	dPack/dt	dMIZ/dt	dPoly/dt	dPack/dt
March	+2,800	+300	+4,100	+1,500	-100	+7,700 <sup>++</sup>
April	-1,400	-1,500	+12,400 <sup>++</sup>	-2,700	-1,400	+14,600 <sup>+++</sup>
May	+2,600 <sup>+</sup>	-2,200	+11,100 <sup>++</sup>	-700	-1,100	+16,400 <sup>+++</sup>
June	0	-1,200	+12,700 <sup>++</sup>	-2,000	-800	+18,600 <sup>+++</sup>
July	+700	-700	+8,200 <sup>+</sup>	-700	-600	+14,200 <sup>+++</sup>
August	+6,900 <sup>+++</sup>	-1,600	+3,400	+500	-900	+12,700 <sup>+++</sup>
September	+4,800 <sup>++</sup>	-1,200	+1,800	-700	-700	+15,100 <sup>+++</sup>
October	+5,400 <sup>+++</sup>	-2,300	+7,300 <sup>+</sup>	+1,100	-1,300	+17,600 <sup>+++</sup>
November	+3,700 <sup>+</sup>	-1,200	+4,400	-700	-1,600	+13,700 <sup>+++</sup>
<b>Bellinghausen/Amundsen Sea</b>						
Month	dMIZ/dt	dPoly/dt	dPack/dt	dMIZ/dt	dPoly/dt	dPack/dt
March	-7,500	-1,500	-2,800	-2,400	-1,700	-7,500
April	-8,600	-800	-3,100	-3,100	-900	-7,700
May	-8,600	-1,200	+2,800	-2,100	-800	-4,600
June	-6,800	-2,600	+8,500 <sup>+++</sup>	-2,100	-500	+1,300
July	-3,500	-2,500	+10,100 <sup>+++</sup>	-700	-700	+4,000
August	-1,200	-700	+7,000 <sup>+</sup>	+500	-200	+2,700
September	+2,600	-500	-300	+1,500 <sup>+</sup>	-200	-100
October	-800	-200	-1,100	-300	-200	-1,800
November	+2,600	+1,000 <sup>++</sup>	-1,400	+1,600	+600 <sup>+</sup>	+300
<b>Weddell Sea</b>						
Month	dMIZ/dt	dPoly/dt	dPack/dt	dMIZ/dt	dPoly/dt	dPack/dt
March	+4,100 <sup>++</sup>	+1,300 <sup>++</sup>	+9,500 <sup>++</sup>	+2,600 <sup>++</sup>	+600 <sup>+</sup>	+13,600 <sup>+++</sup>
April	+1,700	+400	+12,000 <sup>++</sup>	-2,000	+200	+19,200 <sup>+++</sup>
May	-100	-400	+9,400 <sup>++</sup>	-1,500	-600	+14,400 <sup>+++</sup>
June	-2,300	-900	+100	-4,800	-600	+8,800 <sup>++</sup>
July	-2,900	-1,100	-4,800	-4,200	-400	-100
August	-1,700	-700	-5,100	-3,500	-100	+600
September	-200	-600	-100	-2,900	-200	+4,900
October	+4,300	-1,400	-8,800	-3,700	-700	+3,400
November	-2,100	-3,500	-4,700	-6,300	-2,200	+700
<b>Indian Ocean</b>						
Month	dMIZ/dt	dPoly/dt	dPack/dt	dMIZ/dt	dPoly/dt	dPack/dt
March	+2,500 <sup>++</sup>	+300 <sup>+</sup>	+9,500 <sup>++</sup>	+2,100 <sup>++</sup>	+300 <sup>+</sup>	+1,500 <sup>++</sup>
April	+1,500 <sup>+</sup>	+600 <sup>+</sup>	+12,000 <sup>++</sup>	-500	+300	+5,200 <sup>+++</sup>
May	-200	+600 <sup>+</sup>	+9,400 <sup>++</sup>	-1,400	+100	+7,700 <sup>+++</sup>
June	+2,600 <sup>+</sup>	-500	+100	+900	-300	+7,600 <sup>++</sup>
July	+3,500 <sup>+</sup>	-700	-4,800	+100	-100	+7,600 <sup>++</sup>
August	+1,300	-300	-5,100	-1,500	0	+9,900 <sup>+++</sup>



September	+4,600 <sup>+</sup>	-900	-100	+400	-100	+6,700 <sup>++</sup>
October	+1,900	-900	-8,800	-200	-400	+8,600 <sup>++</sup>
November	+2,000	-200	-4,700	-500	-400	+8,700 <sup>++</sup>
<b>Pacific Ocean</b>						
<b>Month</b>	<b>dMIZ/dt</b>	<b>dPoly/dt</b>	<b>dPack/dt</b>	<b>dMIZ/dt</b>	<b>dPoly/dt</b>	<b>dPack/dt</b>
March	+1,100	+400 <sup>+++</sup>	+2,800 <sup>+++</sup>	+1,100 <sup>++</sup>	+600 <sup>+++</sup>	+1,500 <sup>++</sup>
April	-1,400	+800 <sup>+++</sup>	+5,600 <sup>+++</sup>	-2,100	+700 <sup>+++</sup>	+5,200 <sup>+++</sup>
May	-3,000	+800 <sup>++</sup>	+6,100 <sup>+++</sup>	-2,800	+300 <sup>+</sup>	+7,700 <sup>+++</sup>
June	-3,600	+200	+7,000 <sup>+++</sup>	-1,200	-300	+7,600 <sup>++</sup>
July	-1,300	-700	+5,700 <sup>++</sup>	-100	-400	+7,600 <sup>++</sup>
August	-1,500	-300	+2,200	-2,200	-300	+9,900 <sup>+++</sup>
September	-900	-100	+1,400	-2,500	-300	+6,700 <sup>++</sup>
October	-1,200	0	+3,700 <sup>++</sup>	-1,100	-300	+8,600 <sup>++</sup>
November	-3,500	-500	+4,400 <sup>++</sup>	-4,000	-200	+8,700 <sup>++</sup>

842

843



844 **Table 4.** Monthly latitude/longitude corners used for assessment of sea ice conditions on snow petrel  
 845 breeding success.

	April	May	June	July	August	September
Latitude <sub>1</sub>	-65	-65	-65	-65	-65	-65
Latitude <sub>2</sub>	-60	-60	-60	-60	-55	-55
Longitude <sub>1</sub>	90	65	50	35	25	50
Longitude <sub>2</sub>	120	120	120	120	115	140

846

847 **Table 5.** Results of model selection for the relationship between pack ice and MIZ on breeding success  
 848 of snow petrels. Model selection is based on the lowest AIC score, highlighted in gray. The slope of the  
 849 regression is also shown.

Model	Variable	AIC	Slope
Bootstrap	MIZ	931.86	-0.57544
NASA Team	MIZ	887.11	-1.31416
Bootstrap	Pack ice	879.17	-1.04223
NASA Team	Pack ice	927.8	-0.41916

850

851



## 852 List of Figures

853 **Figure 1.** Example of a radial profile from 50 to 90S at -11.60 degrees West on 3 September 1990,  
854 showing the different sea ice classifications found along this transect.

855 **Figure 2:** Samples of ice classification on day 70 (March) and day 273 (September) 2013. Results are  
856 shown for both the NASA Team (top) and Bootstrap (bottom) sea ice algorithms. The MIZ (red)  
857 represents regions of sea ice concentration between 15 and 80% from the outer ice edge, the pack ice is  
858 shown in light purple, representing regions of greater than 80% sea ice concentration. Orange regions  
859 within the pack ice represent coherent regions of less than 80% sea ice concentration, pink areas open  
860 water and green regions of less than 80% sea ice concentration near the Antarctic coastline. Dark blue  
861 represents the ocean mask applied to remove spurious ice concentrations beyond the ice edge.

862 **Figure 3.** Southern hemisphere regions as defined by *Parkinson and Cavalieri* [2012].

863 **Figure 4.** Location of the mean 1981-2010 outer marginal ice edge for both the NASA Team and  
864 Bootstrap algorithms.

865 **Figure 5.** Long-term (1979-2013) seasonal cycle in total Antarctic extent of the consolidated pack ice, the  
866 outer marginal ice zone, polynyas, open pack ice (or broken ice within the pack ice), and inner open  
867 water. There are essentially no scattered ice floes outside of the MIZ. NASA Team results are shown on  
868 the left and the Bootstrap on the right.

869 **Figure 6.** Long-term (1979-2013) seasonal cycle in regional sea ice extent of the consolidated pack ice,  
870 the outer marginal ice zone, polynyas, open pack ice (or broken ice within the pack ice), and inner open  
871 water. Results for the NASA Team algorithm are shown on the left and Bootstrap on the right, and for  
872 the Ross, Bellingshausen/Amundsen, Weddell, Indian and Pacific Oceans.

873 **Figure 7.** Expansion (red) or contraction (blue) of the outer ice edge (top), the width of the marginal ice  
874 zone (middle) and the width of the pack ice from 1979 to 2013 during the month of September.

875 **Figure 8.** Daily trends (1979 to 2013) in the consolidated pack ice, the outer MIZ and potential coastal  
876 polynyas for the entire Antarctic sea ice cover for the NASA Team (left) and Bootstrap (right) algorithms.  
877 Trends are provided in  $10^6 \text{ km}^2 \text{ a}^{-1}$ .

878 **Figure 9.** Daily (1979-2013) trends in regional sea ice extent of the consolidated pack ice (top), the outer  
879 marginal ice zone (middle) and potential coastal polynyas (bottom). Results for the NASA Team  
880 algorithm (left) and Bootstrap (right) are shown as a function of longitude. Trends are provided in  $10^6$   
881  $\text{km}^2 \text{ a}^{-1}$ . Note the difference in color bar scales.

882 **Figure 10.** Time-series of seasonal mean JJA (top), SON (middle) and MAM (bottom) marginal ice zone  
883 (left) and consolidated pack ice (right) for both sea ice algorithms; NASA Team is shown in red, Bootstrap  
884 in black. Shading represents one standard deviation. Note the difference in y-axis between the pack ice  
885 and the MIZ plots.

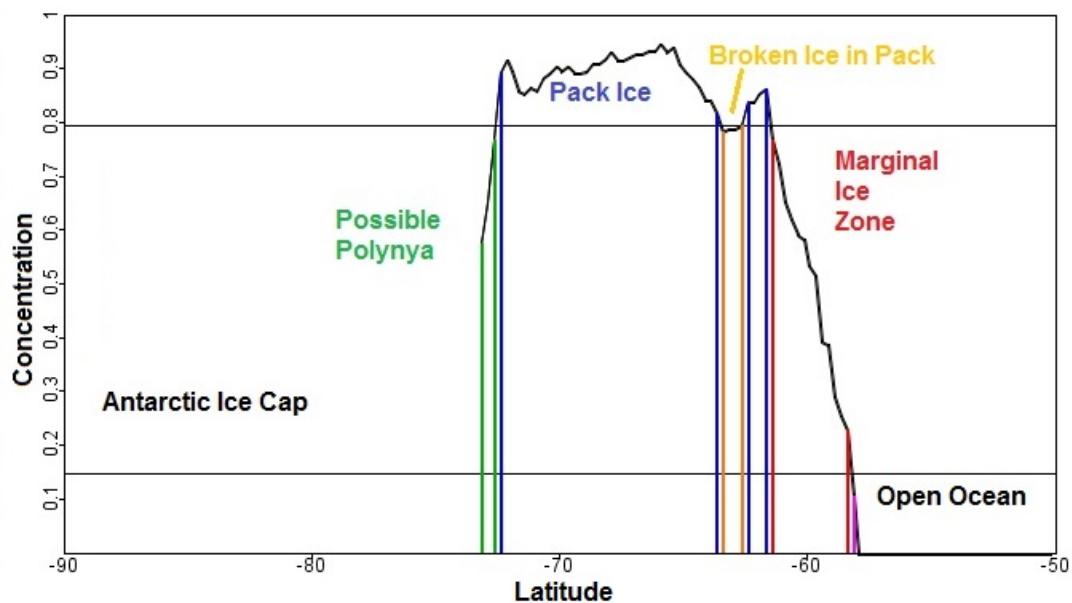


886 **Figure 11.** Breeding success of snow petrel (top) and effect of the Bootstrap pack ice on the breeding  
887 success of snow petrels (bottom).

888



889



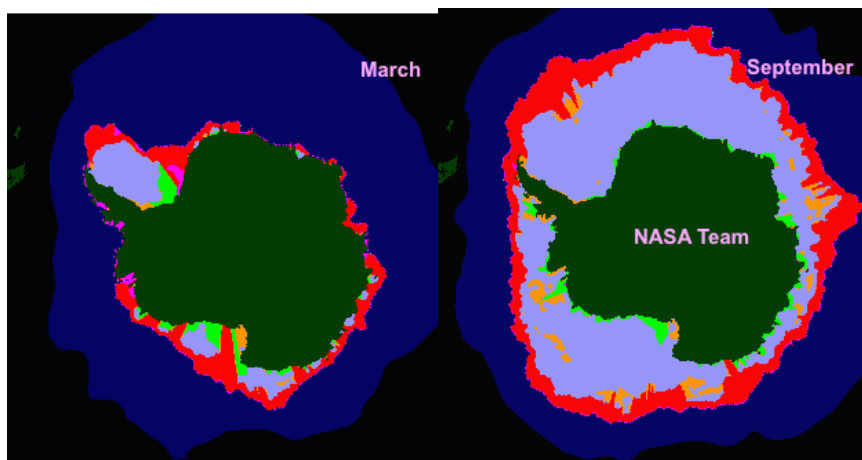
890

891 **Figure 1.** Example of a radial profile from 50 to 90S at -11.60 degrees West on 3 September 1990,  
892 showing the different sea ice classifications found along this transect.

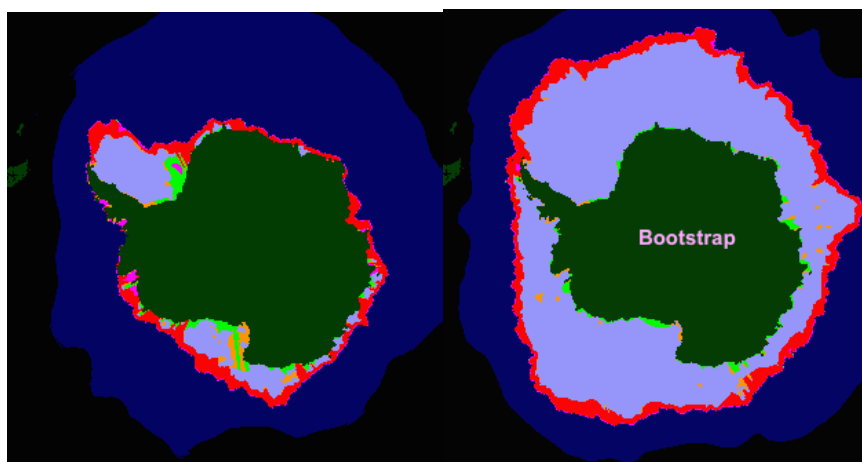
893



894

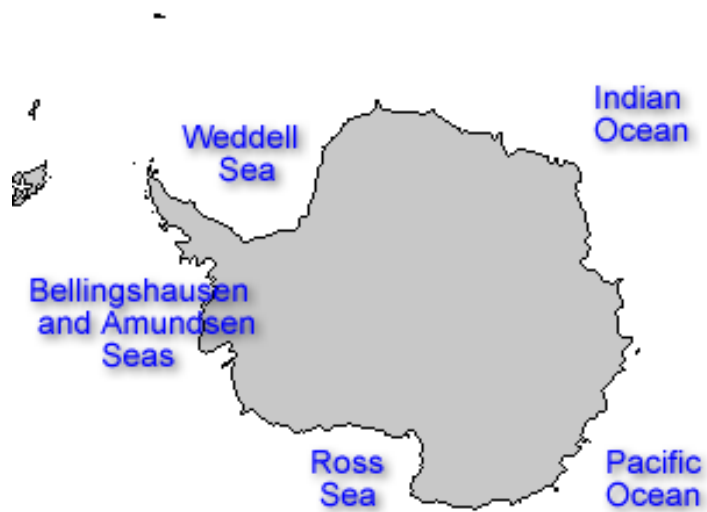


895



896 **Figure 2:** Samples of ice classification on day 70 (March) and day 273 (September) 2013. Results are  
897 shown for both the NASA Team (top) and Bootstrap (bottom) sea ice algorithms. The MIZ (red)  
898 represents regions of sea ice concentration between 15 and 80% south of the outer ice edge (defined by  
899 the ocean mask) and north of the pack ice. The pack ice is shown in light purple, representing regions of  
900 greater than 80% sea ice concentration. Orange regions within the pack ice (and away from the  
901 coastline) represent ‘broken ice areas’, coherent regions of less than 80% sea ice concentration. Pink  
902 areas are open water (SIC < 15%) areas detected south of the ocean mask but north of the coastline, and  
903 light green areas of less than 80% sea ice concentration extending from the Antarctic coastline are  
904 potential coastal polynyas. Dark blue represents the ocean mask applied to remove spurious ice  
905 concentrations at and beyond the ice edge.

906

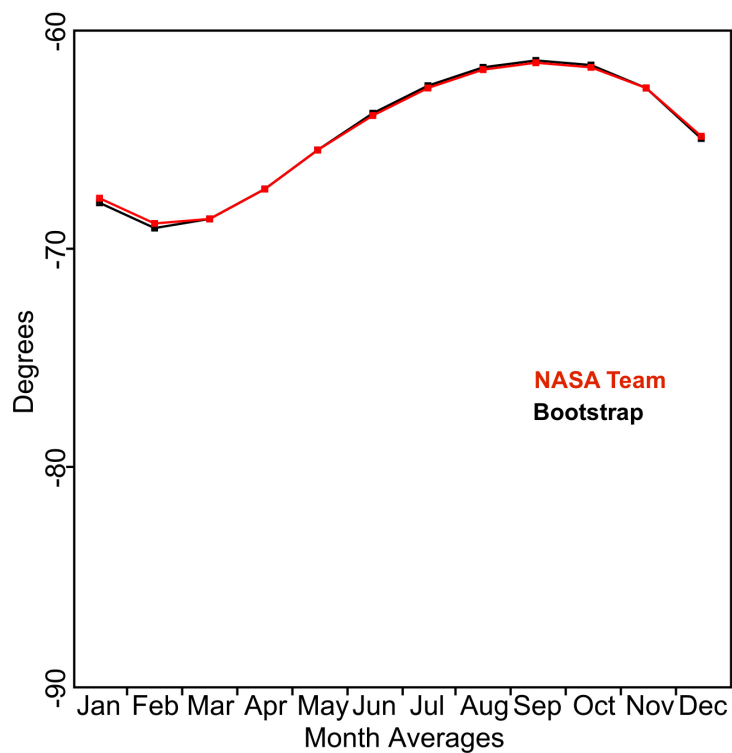


907

908 **Figure 3.** Southern hemisphere regions as defined by *Parkinson and Cavalieri* [2012].

909

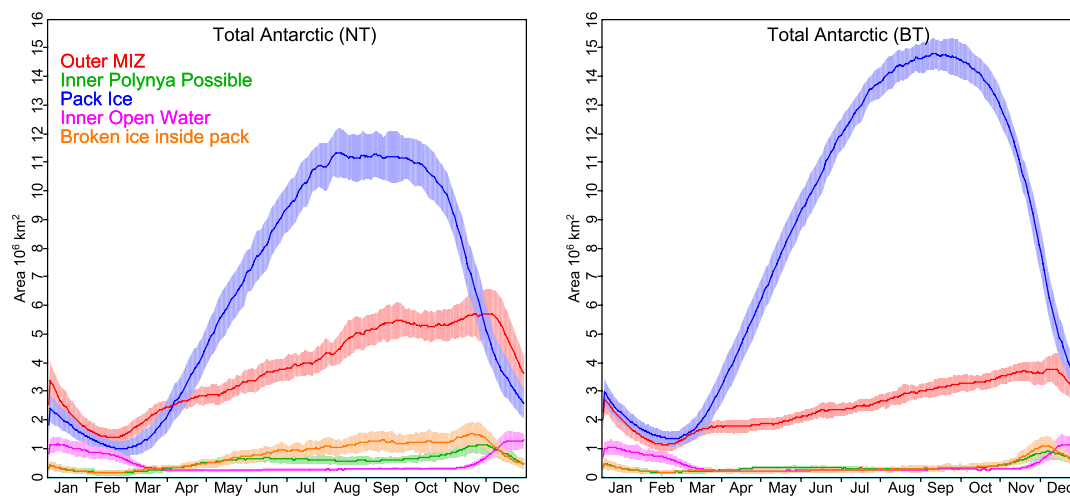




910

911 **Figure 4.** Location of the mean 1981-2010 outer marginal ice edge for both the NASA Team and  
912 Bootstrap algorithms.

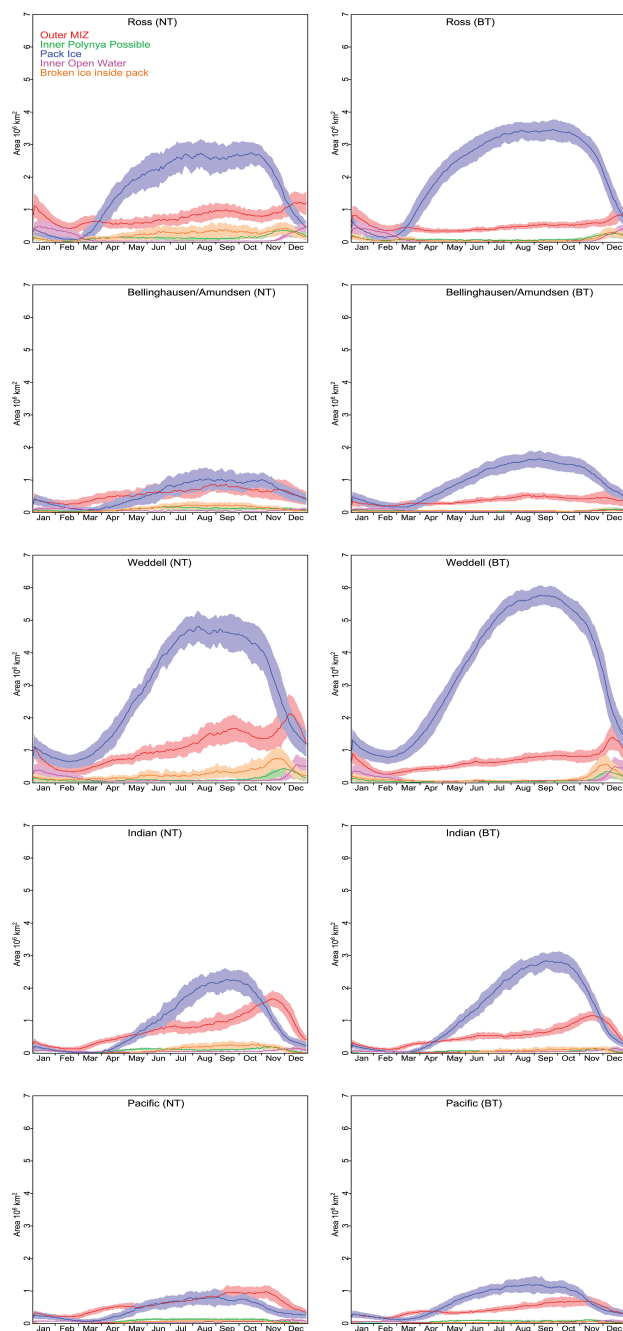
913



914  
915 **Figure 5.** Long-term (1979-2013) seasonal cycle in total Antarctic extent of the consolidated pack ice, the  
916 outer marginal ice zone, polynyas, broken ice within the pack ice, and inner open water. There are  
917 essentially no scattered ice floes outside of the MIZ. NASA Team results are shown on the left and the  
918 Bootstrap on the right.

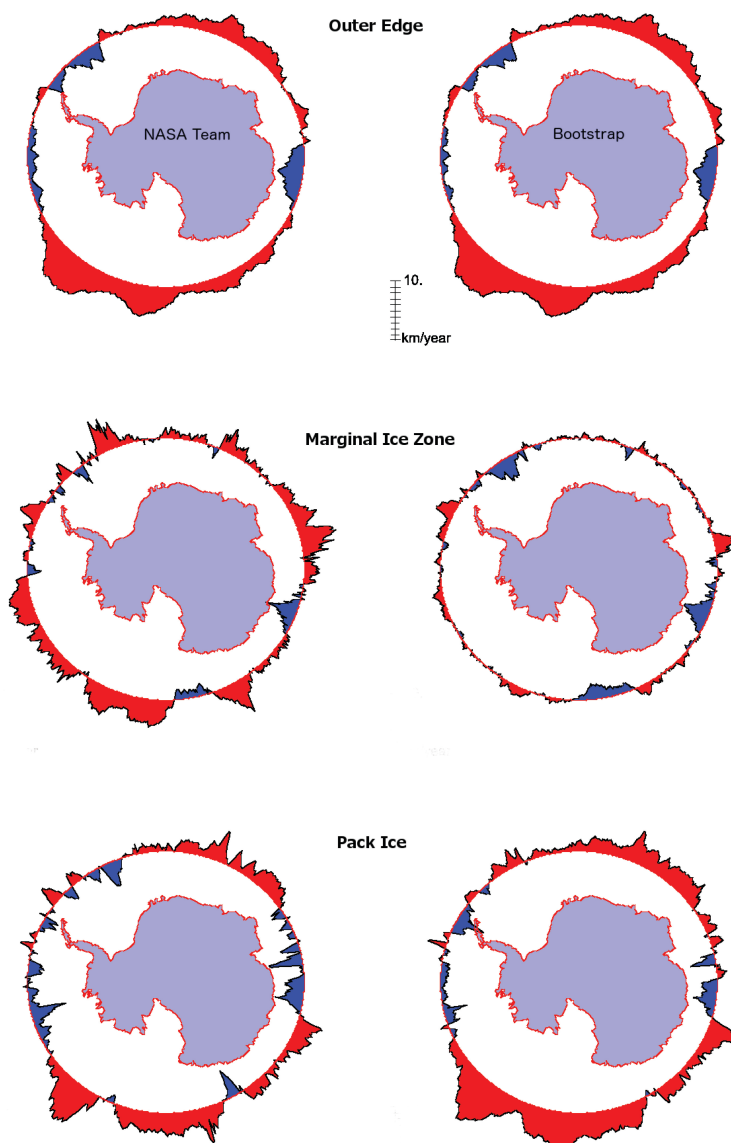
919

920

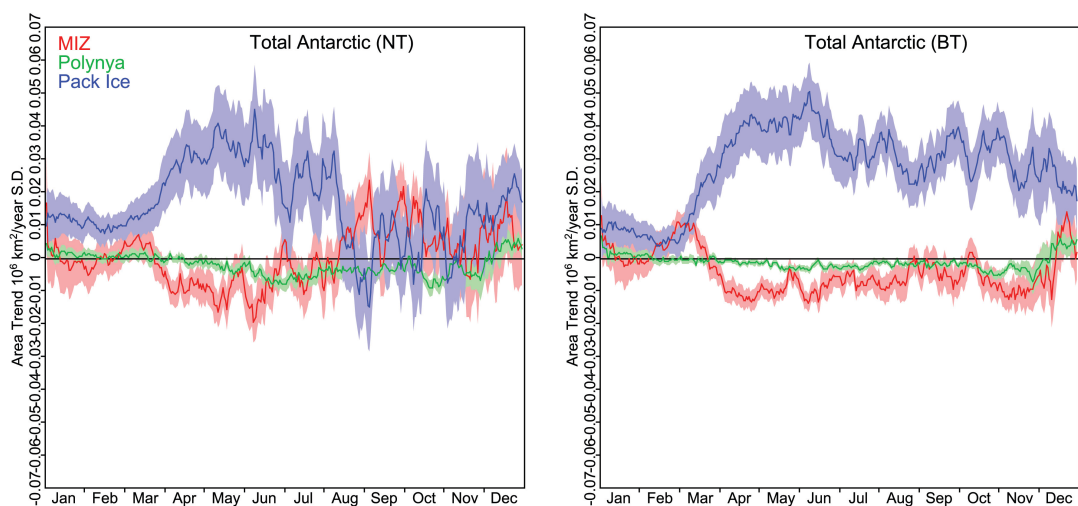


921

922 **Figure 6.** Long-term (1979-2013) seasonal cycle in regional sea ice extent of the consolidated pack ice,  
923 the outer marginal ice zone, polynyas, broken ice within the pack ice, and inner open water. Results for  
924 the NASA Team algorithm are shown on the left and Bootstrap on the right, and for the Ross,  
925 Bellinghausen/Amundsen, Weddell, Indian and Pacific Oceans.



926  
927 **Figure 7.** Expansion (red) or contraction (blue) of the outer ice edge (top), the width of the marginal ice  
928 zone (middle) and the width of the pack ice from 1979 to 2013 during the month of September.



929

930 **Figure 8.** Daily trends (1979 to 2013) in the consolidated pack ice, the outer MIZ and potential coastal  
931 polynyas for the entire Antarctic sea ice cover for the NASA Team (left) and Bootstrap (right) algorithms.  
932 Trends are provided in  $10^6 \text{ km}^2 \text{ a}^{-1}$ .

933

934

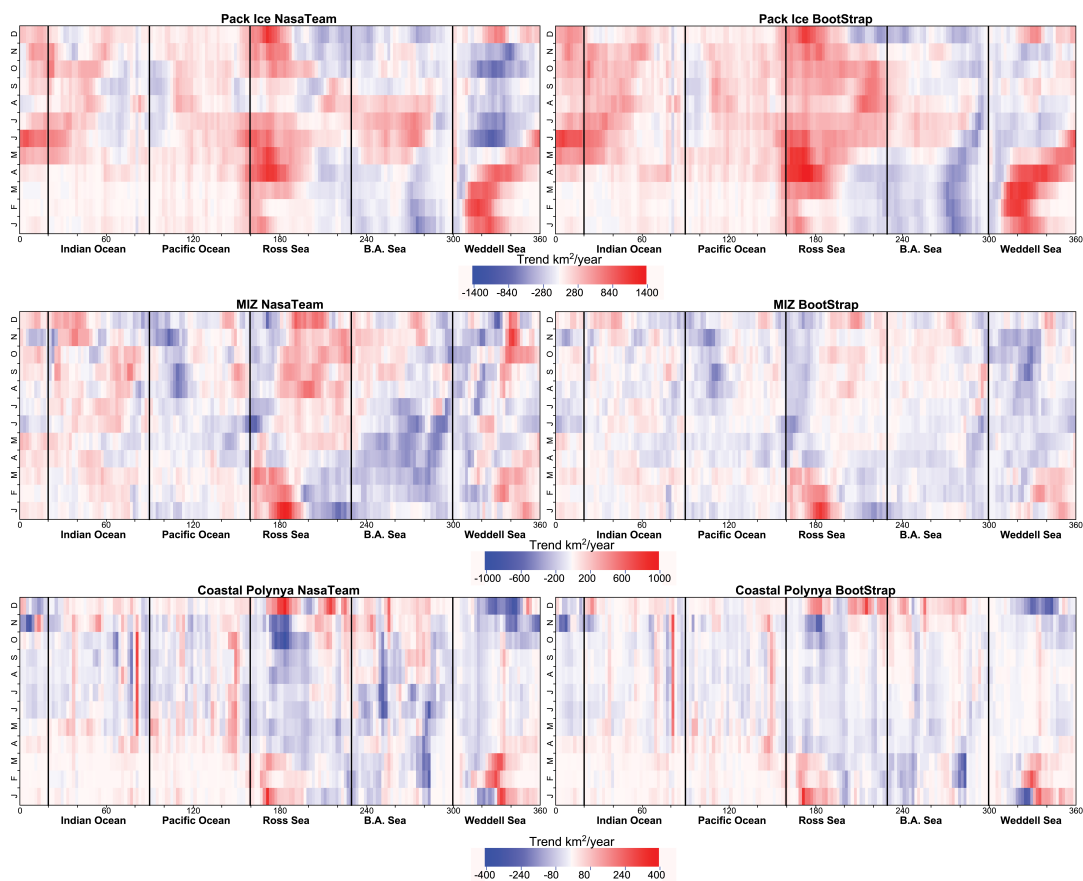
935

936

937



938

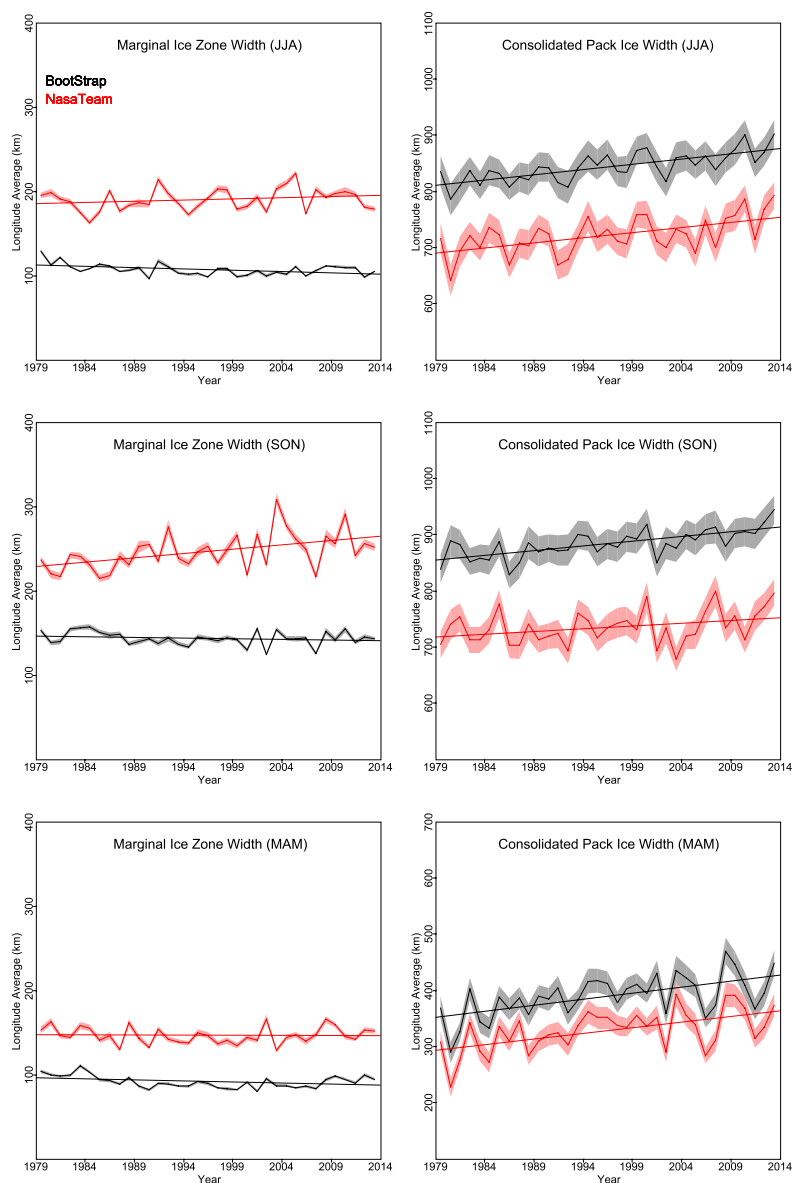


939

940 **Figure 9.** Daily (1979-2013) trends in regional sea ice extent of the consolidated pack ice (top), the outer  
941 marginal ice zone (middle) and potential coastal polynyas (bottom). Results for the NASA Team  
942 algorithm (left) and Bootstrap (right) are shown as a function of longitude. Trends are provided in  $10^6$   
943  $\text{km}^2 \text{a}^{-1}$ . Note the difference in color bar scales.

944

945



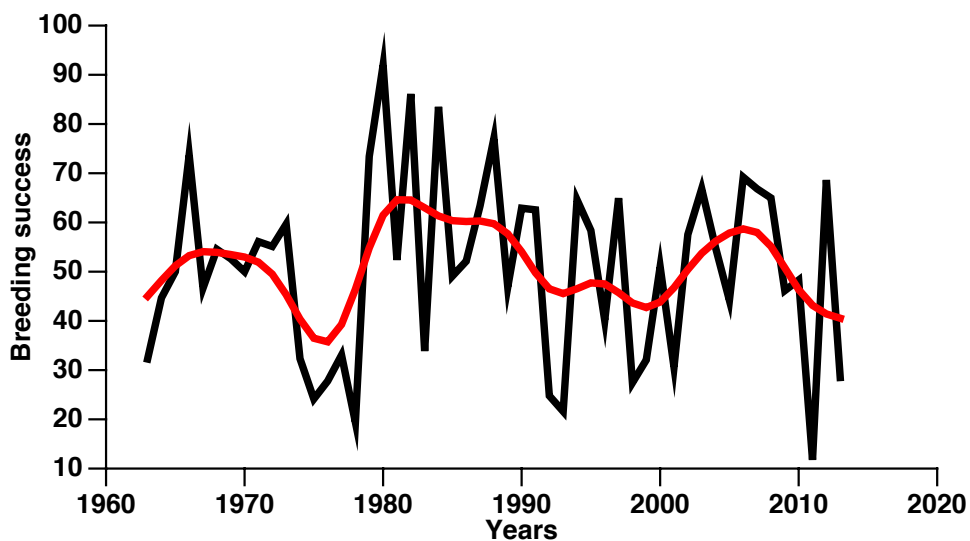
946

947 **Figure 10.** Time-series of seasonal mean JJA (top), SON (middle) and MAM (bottom) marginal ice zone  
 948 (left) and consolidated pack ice (right) for both sea ice algorithms; NASA Team is shown in red, Bootstrap  
 949 in black. Shading represents one standard deviation. Note the difference in y-axis between the pack ice  
 950 and the MIZ plots.

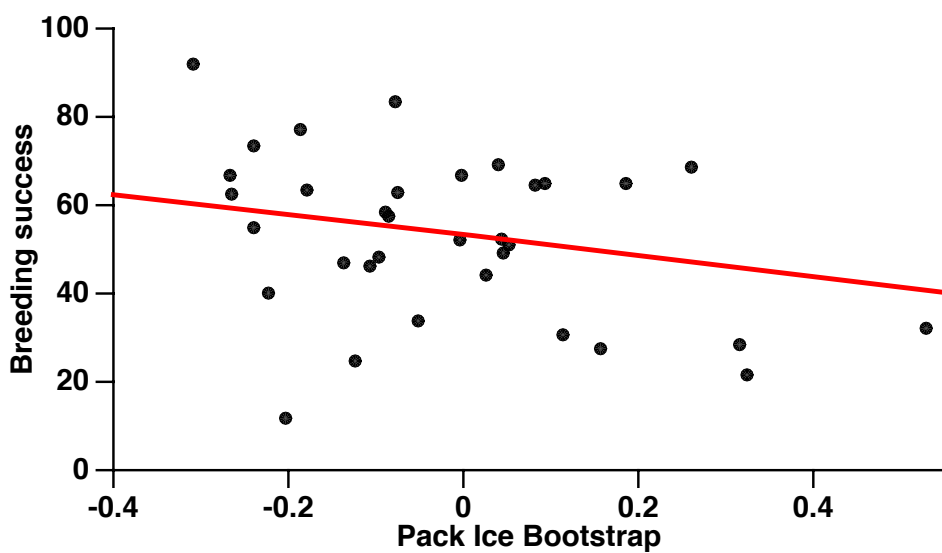
951



952



953



954

955 **Figure 11.** Breeding success of snow petrel (top) and effect of the Bootstrap pack ice on the breeding  
956 success of snow petrels (bottom).

957

958

959